sciendo
Austrian Journal of Earth Sciences | Vienna | 2025 | Volume 118 | 115–132 | DOI: 10.17738/ajes.2025.0006

Fault mirrors in the process zone of a seismogenic fault (Karawanks, Eastern Alps)

Stefanie J. Koppensteiner[1,2*], Harald Bauer[2], Bernhard Grasemann[1], Lukas Plan[2,3], Ivo Baroň[4]

[1)] Department of Geology, Josef-Holaubek-Platz 2, 1090 Vienna, Austria
[2)] Speleological Society of Vienna and Lower Austria, Obere Donaustraße 97/1/61, 1020 Vienna, Austria
[3)] Karst and Cave Group, National History Museum, Burgring 7, 1010 Vienna, Austria
[4)] Institute of Rock Structure and Mechanics of the Czech Academy of Sciences, v. v. i., V Holešovičkách 94/41, 182 09 Praha, Czech Republic
[*)] Corresponding author: s.j.koppensteiner@gmail.com

Keywords: Fault mirror, Polished slickenside, Seismic slip, Periadriatic Fault, Obir Caves, Eastern Alps

Abstract

Square centimetres sized polished fault surfaces are exposed in the vicinity of a seismic fault in the Obir Caves (Northern Karawanks, Carinthia, Austria). Microtectonic studies reveal that contrary to published natural and experimental fault mirrors, these small-scale faults record almost no displacement. Based on our findings, we propose a new process, in which during the passage of seismic waves, small shaking movements along the slip surfaces with hardly any offset caused the development of polished slickensides. The Obir Caves in the Hochobir massif are located just north of the seismogenic ESE striking, dextral Periadriatic Fault System, which forms the boundary between the Eastern and the Southern Alps. The cave was partially formed along the sinistral Obir Fault, close to which a high density of centimetres to decimetres long polished slickensides have been observed. The knife-sharp slip surfaces are associated with millimetre to centimetre thin layers of ultracataclasites, in either hardly deformed or protocataclastic rocks. The highly mature ultracataclasites record angular to rounded clasts, which are truncated along the polished slickensides, but clear kinematic indicators are generally missing. Injection of the ultracataclasites into the protocataclastic host rocks along millimetre-wide apophysis can be locally observed. Some of the older cataclasite generations are overprinted by stylolites and calcite veins suggesting dissolution precipitation processes after cataclastic flow. The only several centimetres-long polished slickensides with varying properties and orientations cannot have accumulated large displacements but the observed microstructures as well as the geological position in an area with several active faults suggest that the investigated fault surfaces in the Obir Caves formed during seismic slip.

1. Introduction

Fault mirrors, also known as mirror slickensides or polished slickensides, are naturally polished light-reflective slip surfaces. They occur mostly in carbonate rocks of the shallow crust but have also been reported in tourmaline (Viti et al., 2016). Research on natural fault mirrors in seismically active areas (Smith et al., 2011; Siman-Tov et al., 2013; Kuo et al., 2016; Smeraglia et al., 2017; Ohl et al., 2020) or on laboratory scales (Fondriest et al, 2013; Siman-Tov et al., 2015; Tesei et al., 2017) reported highly-reflective fault surfaces with grooves and gouge striations as well as microstructures such as clast-cortex grains, truncated grains, ultracataclastic sub-layers and bulbous protrusion of ultracataclastic material as evidence for fluidisation. Opposing to these studies, friction experiments under aseismic velocity conditions of Verberne et al. (2014) did also result in the formation of patchy, mirror-like surfaces. The authors concluded that polished slickensides in calcite(-rich) fault rocks cannot be used as a reliable indicator for palaeoseismic slip. Pozzi et al. (2018) integrat-

ed mechanical data and microstructural observations to develop a new conceptual model of mirror slickensides throughout the weakening history of calcite gouges sheared at seismic velocities. As a result, they presented polished slickensides as a marker of rheological contrast, across which an extremely sharp strain gradient was observed. They concluded that mirror slickensides are not frictional slip surfaces in the classical sense, but seismic slip velocities and coinciding shear heating make their formation more likely. All these investigations suggest that different deformation mechanisms may lead to similar structures, so that fault mirrors generally cannot be defined as being formed at seismic slip rates (Billi and Di Toro, 2008; Han and Hirose, 2012; Rempe et al., 2014; Piane et al., 2017).

This study focuses on understanding the processes responsible for the formation of small-scale mirror slickensides by integrating microstructural observations with field data collected both within and around the Obir Caves (Northern Karawanks, Austria). Our findings culminate in a conceptual model proposing that small-scale fault mirrors are structures formed in close proximity to an earthquake's epicentre.

2. Geological and tectonic setting

The main tectonic structure of the study area is the seismically active Periadriatic Fault System. With its 700 km in length, it is a first-order tectonic boundary within the Alps (Schmid et al., 1989; Márton et al., 2006). This major fault was described by Suess (1901) who interpreted the structure as the suture between Europe and Africa (Suess, 1901; Clar, 1953; Kober, 1955). More recent works place the origin of the Periadriatic Fault System in the early Lower Cretaceous and the formation of its current form in the Oligocene with the intrusion of Periadriatic plutons (Sprenger, 1996; Mancktelow et al., 2001; Müller et al., 2001). On the contrary, Schönlaub and Schuster (2015), suggest a Late Jurassic origin with several reactivation periods.

The amount of right lateral displacement along the Periadriatic Lineament has been discussed for decades and estimates range between 300 and 500 km (e.g. Laubscher, 1973; Bögel, 1975; Tollmann, 1977; Bauer and Schermann, 1984; Frisch et al., 1998). Vrabec et al. (2006) pointed out that a dextral separation of 300–500 km of formerly assumed palaeogeographic markers in the Paleozoic-Mesozoic as well as Cenozoic (Paleogene and Neogene) along the Periadriatic Fault are not realistic.

The fault zone is up to several kilometres wide and comprises elongated, fault-parallel shear lenses and strike-slip duplexes (Fig. 1). These duplexes consist of strongly deformed Paleo- to Cenozoic rocks (Vrabec et al., 2006). In the area of interest, the Periadriatic Fault System divides the Karawanks mountain range into the Northern and Southern Karawanks. The study area is located 4 km north to this division in the Northern Karawanks within a transpressional zone of the main fault strand. The investigated Obir Caves are developed near the mining area of the Untere Schäfleralm on the eastern slopes of the Hochobir mountain (summit: 2139 m a.s.l.). This mountain range is part of the Drauzug-Gurktal Nappe System (Krainer 1998; Froitzheim et al., 2008) and is mainly built up of Middle Triassic limestone and dolostone of the Wetterstein Formation. It is dissected by the NE-SW striking sinistral Obir Fault system offsetting fluvial channels and forming a system of scarps and lineaments in the recent topography, which was subsequently affected by a younger deep-seated gravitational slope deformation (Baroň et al., 2019a, 2019b, 2022a).

The Obir Caves consist of approximately a dozen caves with a total length of 5 km and were discovered during the mining of lead and zinc ore (Jahne, 1929). Parts of the caves and mines were developed as show caves. The caves have a hypogenic origin due to rising carbonic acid and were formed below the water table with later localized overprinting above the water table (Spötl et al., 2023). The genesis of the cave passages is controlled by faults of the Obir Fault System. Offset of the original dissolution morphology and deformed speleothems in several parts of the caves indicate reactivation of the fault and reveal the micro-kinematic activity to the present day (Baroň et al., 2019a; 2019b, 2022a). In addition to three potentially strong prehistoric earthquakes there is evidence of at least 41 cm of sinistral fault slip, 3 cm of dextral oblique reverse fault slip and further speleothem damage occurring in several events over the last 43 ka in the Obir Caves (Baroň et al., 2022a).

The main investigation site of this study is located in the part of the Obir Caves known as Wartburg Cave, where nearly parallel galleries formed along NE-SW and ENE-WSW trending fault planes. The exact location of the exposure with the much smaller, naturally polished slickensides is shown in Figure 2.

3. Methods

It is noted that the terms slip surface and slip zone are used according to Smith et al. (2011), who followed the classification scheme of Sibson (1977): the slip surface corresponds to the fault plane itself, which is marked by surface striae and polished slickensides; the slip zone lies immediately below the slip surface and contains variably developed fault rock material.

In course of this study, a total of 41 polished slickensides were documented in the field. 18 of them were situated in the Wartburg Cave from which we took nine oriented samples. Besides spatial measurements of their orientation, the following main characteristics of polished slickensides were documented: polishing grade, size and the occurrence of truncated grains (size and number). The visual classification of the polishing grade of the fault surface was done in five classes: 1 – no visible polished spots (none-reflective), 2 – isolated square millimetre sized polished spots, 3 – isolated as well as connected square centimetre sized polished spots,

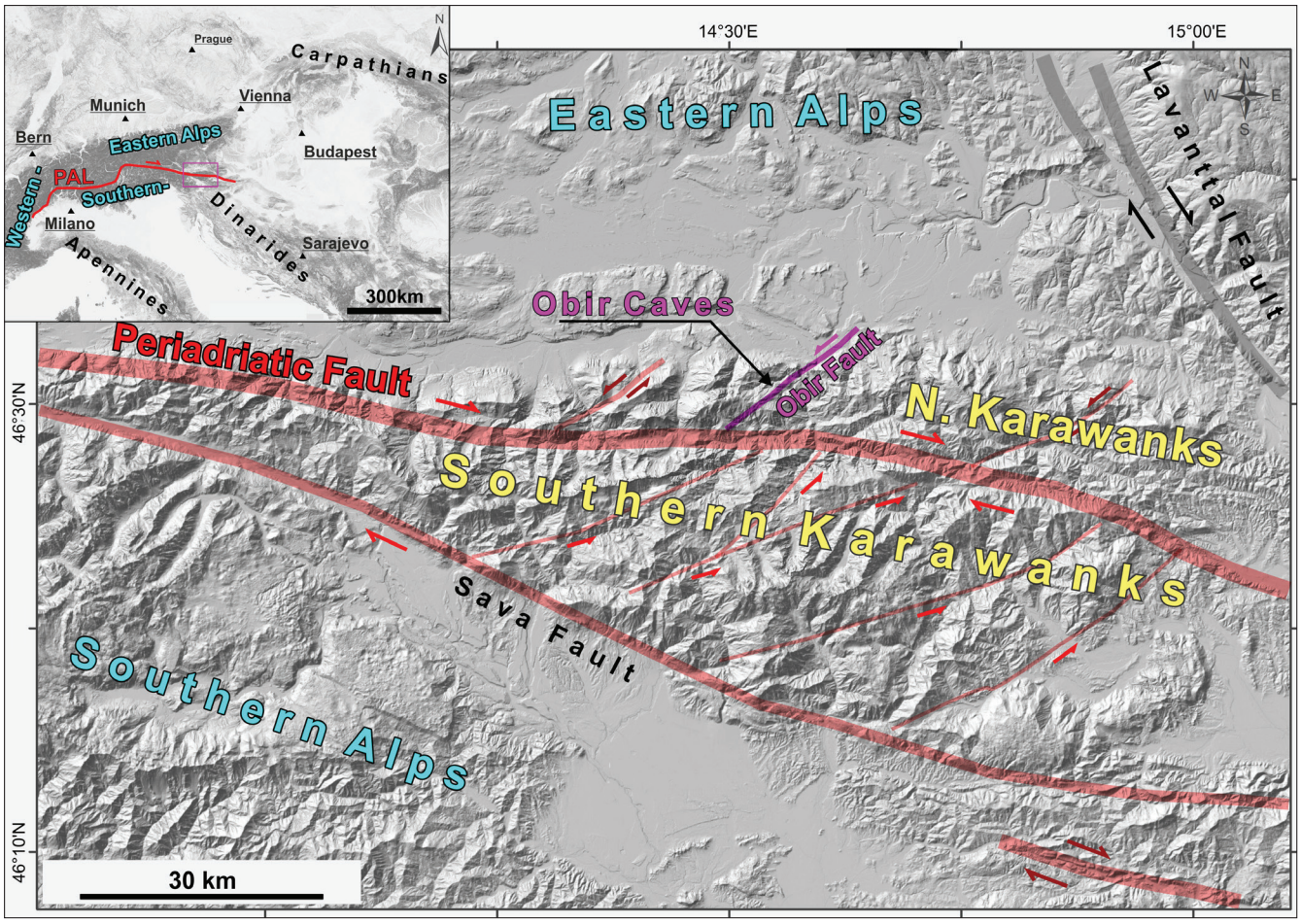

Figure 1: Tectonic setting of the study area shown on a map of the Eastern and Southern Alps transition. Thick lines indicate the dextral Periadriatic, Sava and Lavanttal Fault systems. Insert shows the location of the greater study area, the Karawanks (magenta box) within Central Europe (Map based on SRTM USGS/NASA and 10-m Lidar DEM; after Baroň et al. 2022a, 2022b).

4 – mostly polished with isolated non-polished millimetre sized spots, 5 – the whole fault surface is polished and highly reflective.

Twelve polished thin sections with a thickness of 30 µm were prepared from seven of the oriented samples. Due to the high porosity of the rock, all samples were impregnated with resin prior to cutting perpendicular to the polished slickenside and parallel to the lineation. Three thin sections were selected to identify the cataclastic maturity of the deformed bedrock. This was done based on the various shapes of the grains bigger than 1.3 x 1.7 mm, whereas angular ones indicate a low and rounded ones a high grade of maturity, i.e. deformation. In a first subdivision, the grains were categorised into three groups: angular, rounded and subrounded/subangular. A further subdivision was made when the grains were broken into fragments or showed additional offset. Apart from that a group called "highly fractured" was used to delimit areas of grain fragments, which could be easily put back together to their original form.

The stages of cataclastic deformation were identified for some samples. Based on the works of Sibson (1977), Loucks (1999), Woodcock and Mort (2008) and Billi (2010) six stages of cataclastic maturity were distinguished: 0 – undeformed bedrock, I – angular grains show little evidence of rotation but are separated by thin ultracataclastic seams, II – greater separation of fine-grained matrix between grains + more rotation + many jigsaw fit fragments, III – fragmented clasts can hardly be reassembled to their original form + more fine-grained matrix, IV – fragmented clasts cannot be reassembled + fine-grained matrix and clasts have roughly the same share, V – less fragmented clasts that cannot be reassembled + ultracataclastic matrix exceeds the proportion of clasts.

High-resolution digital microscope images (Keyence Digital VHX-5000) were automatically stitched to maps of the thin sections. 3D surface topography models of three polished hand specimen were calculated from max. 200 pictures per sample at a step size between 0.1 and 0.5 µm.

The mineralogy of the rock was investigated by X-ray diffraction (XRD; Panalytical X'Pert Pro diffractometer, Department of Geology, University of Vienna) on powder from one of the samples.

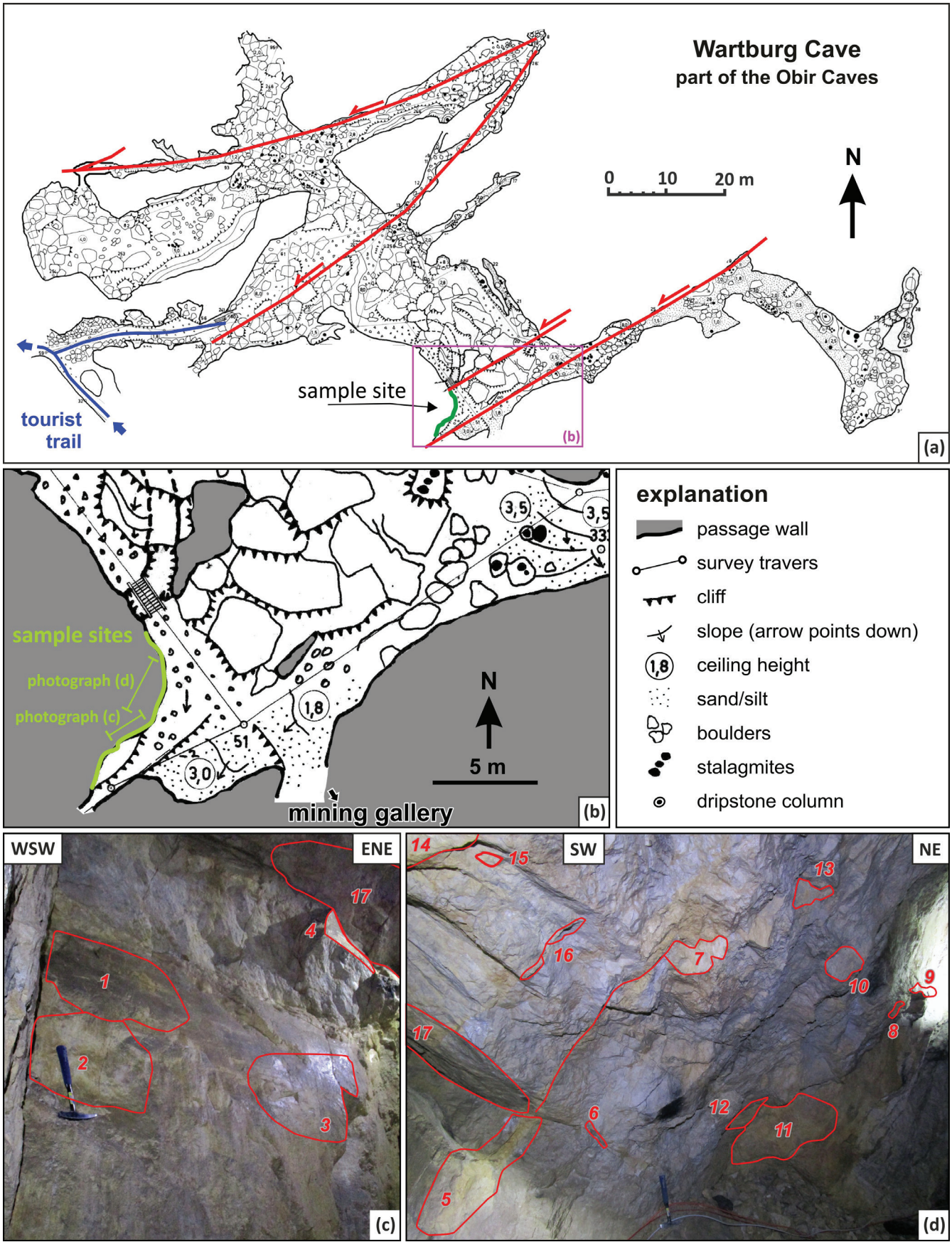

Figure 2: (a) Map of the Wartburg Cave, modified from Thaler et al. (1970) and Baroň et al. (2019a). Red lines mark fault planes observed in the Obir Fault System. The sample site is marked in green. **(b)** Detail of the map with the investigated exposure and the location of the photographs showing the observed slickensides. **(c)** and **(d)** Photographs documenting the polished slickensides (OB1 to OB18).

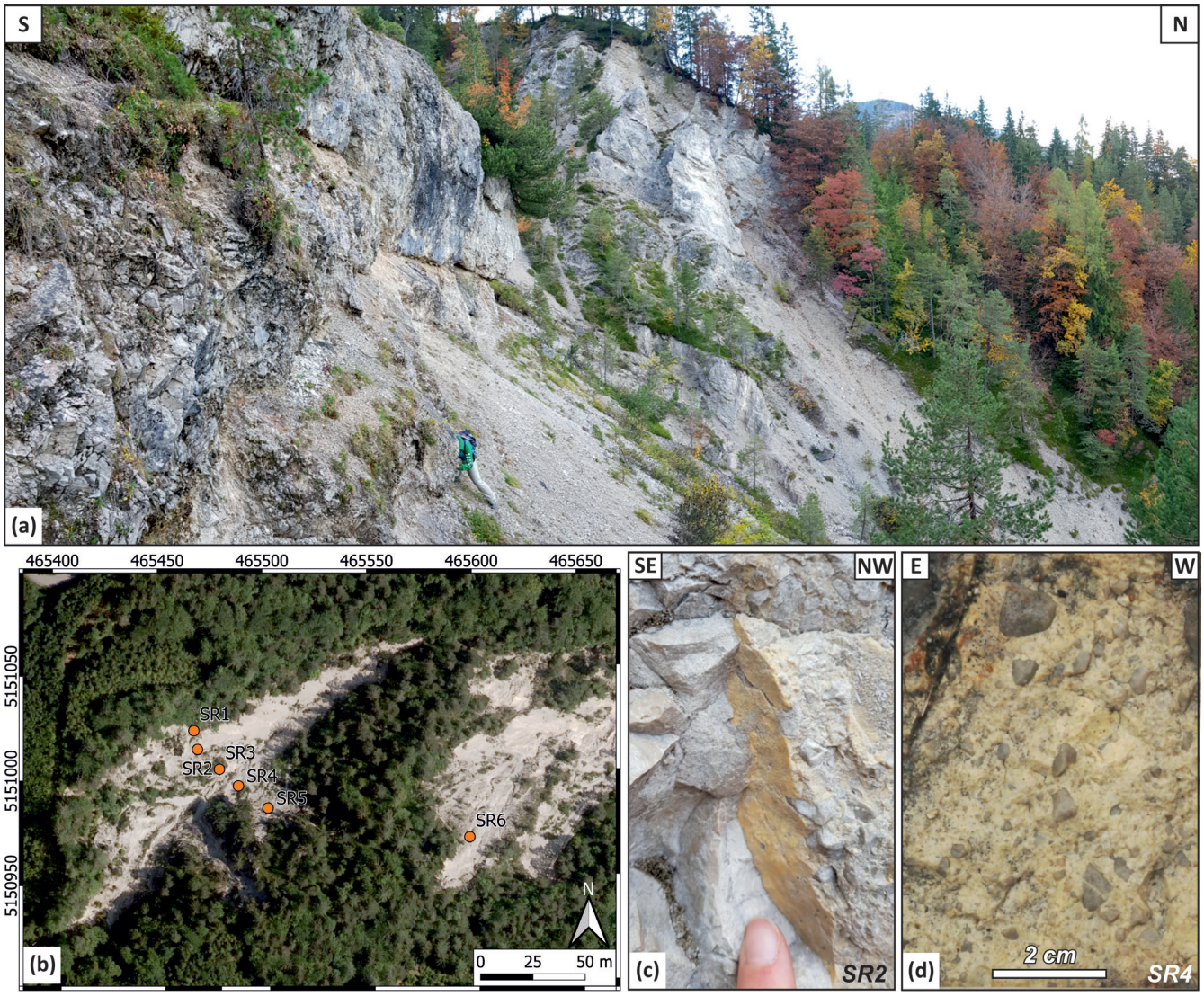

Figure 3: (a) Overview of the cliffs along which the investigated outcrops of the western scree of shattered carbonate rock are located. Photo was taken at outcrop SR5. **(b)** Orthophotograph of the screes of shattered rock 1 and 2 (Source: geoland.at). Orange dots show locations of measurements. Coordinate system: UTM 33N. **(c)** Curved polished slickenside from outcrop SR2 on yellowish cataclasites. **(d)** Left boundary of a yellow cataclastic band in SR4. Small clasts show maximum apparent lengths of 4 x 10 mm. Some have intragranular fractures filled with the surrounding yellowish matrix.

4. Results

4.1. Field observations

4.1.1. Eastern slope of Hochobir Mountain

At the surface outcrops (1) along the gravel road from Zauchen to the entrance of the Obir Caves, (2) along steep rock cliffs above screes of shattered carbonate rock, which are located to the northeast of the tourist entrance of the Obir Caves, (3) around the adit mouth of "Markusstollen", where the guided tour through the Obir Caves ends, and (4) near the entrance of the mining tunnel directly above the "Markusstollen" were investigated. The source areas of the screes consist of highly fractured steep rock cliffs (Fig. 3a, b). Fault mirrors mostly occurred at the boundary of fault zones, where yellowish ultracataclastic material appeared as bands within the bedrock (see Fig. 3c, d).

The stereographic projection of the fault surfaces shows that most of them are steeply dipping (Fig. 4a). There is a weak preferred dip direction towards SE and NW. The orientation of the main fault surface observed in the mining tunnel above Markusstollen is 296/80 (dip direction/dip). Most of the investigated fault surfaces showed polishing grades around 2. Their diameters were in a range of some centimetres up to several metres. The variation of the degree of polishing of slickensides within an outcrop was random and in Figure 4a the colour-coded polishing degree shows no correlation between the dip direction of the surfaces and their polishing grades.

4.1.2. Wartburg Cave

The sampling site is located in the southern part of the Wartburg Cave about 40 m beneath the ground surface

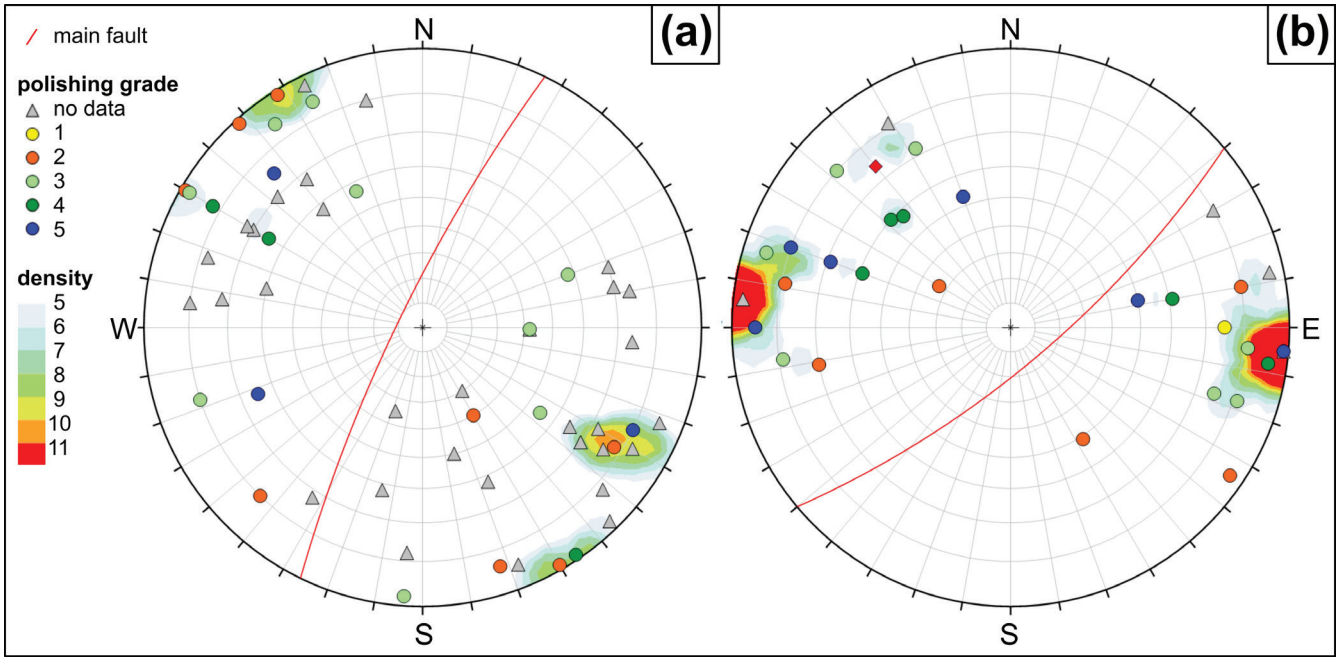

Figure 4: Pole points of all fault planes measured **(a)** at the surface and **(b)** in Wartburg Cave. Colour according to their polishing grade (projection on lower hemisphere, density calculation: Fisher distribution). If a surface has more than one polishing grade, the highest grade is shown. The polishing grade could not be determined for all surfaces. The main faults (a) from the mining tunnel and (b) of the Wartburg Cave are shown as great circles.

(Fig. 2). There a block with a diameter of 5 m is situated between two strands of the Obir Fault System (hereafter referred to as "main faults"). The southern bordering main fault strikes ENE-WSW with a dip angle of around 70 degrees. A post-speleogenetic sinistral offset of about 13 cm was described in Baroň et al. (2019a). The northern main fault strikes in a nearly parallel direction but wasn't accessible for direct investigation. The block is exposed NE to SE and hosts numerous secondary faults, which exhibit polished surfaces. On average, the fault planes on these sub-surface exposures appeared more polished than on the surface outcrops which is ascribed to limited atmospheric weathering processes inside the cave.

Eighteen slickensides were documented (Fig. 2) and from four of them we took nine oriented hand samples containing slickensides with different properties (e.g., size, colour, polishing grade). Six of them were taken from sample point OB5 (Fig. 2d), where more polished surfaces appeared underneath as the first sample was taken. While most samples show fault mirrors localized in cataclasites, sample site OB10 showed the polished bedrock. Some hand samples are almost completely covered with fault mirrors, e.g. sample OB5.3, which has the most polished slickensides of all. It was collected from a minor fault zone, which appeared as an up to 40 cm wide band consisting mostly of ultracataclasites (in Fig. 2d its location is shown as a connecting line between sampling points OB5 and OB7). The sample is shown in Figure 5, where different polished slickensides are mapped in different colours and lineations are indicated as red lines.

Most of the fault surfaces at the exposure in Wartburg cave are steeply dipping (Fig. 4b). The weakly preferred orientations of the slip surfaces show strike directions between WNW and ENE. The orientation of the main fault observed in the cave is 140/74. The colouring of the pole points shows no distinct correlation between orientation and their polishing grades. Comparing the macroscopic observations reveals distinct differences between the individual polished slickensides. The size of the slip surfaces varies from a few cm up to meters in diameter. The spatial orientation of the slip surfaces and slicken lineations do not record strong preferred orientations. Adjacent polished slickensides can show different orientation and lineation directions (Fig. 5). The polishing grade varies from 1 to 5 (see section 3), whereas the proportion of polished surface area goes hand in hand with reflectivity. The shape of the slip surfaces can be straight, curved, corrugated or rarely rough. Varying combinations of these properties occur at the exposure. Most of the slip surfaces are found in ultracataclastic fault rocks with dark-yellow, beige-yellow, pale-yellow, white and reddish-brown colours of the polished slickensides. They predominantly show grains truncated by fault mirrors. These truncated grains differ in size (up to a few mm) and distribution (Fig. 6a, b).

4.2. Microstructures

The samples selected for thin section analysis exhibit polished slickensides with a predominant polishing grade of 3 to 5 (cf. sections 3 and 4.1). Most thin sections show knife-sharp slip surfaces, although some are slightly curved or corrugated (Figs. 7 and 8a). One

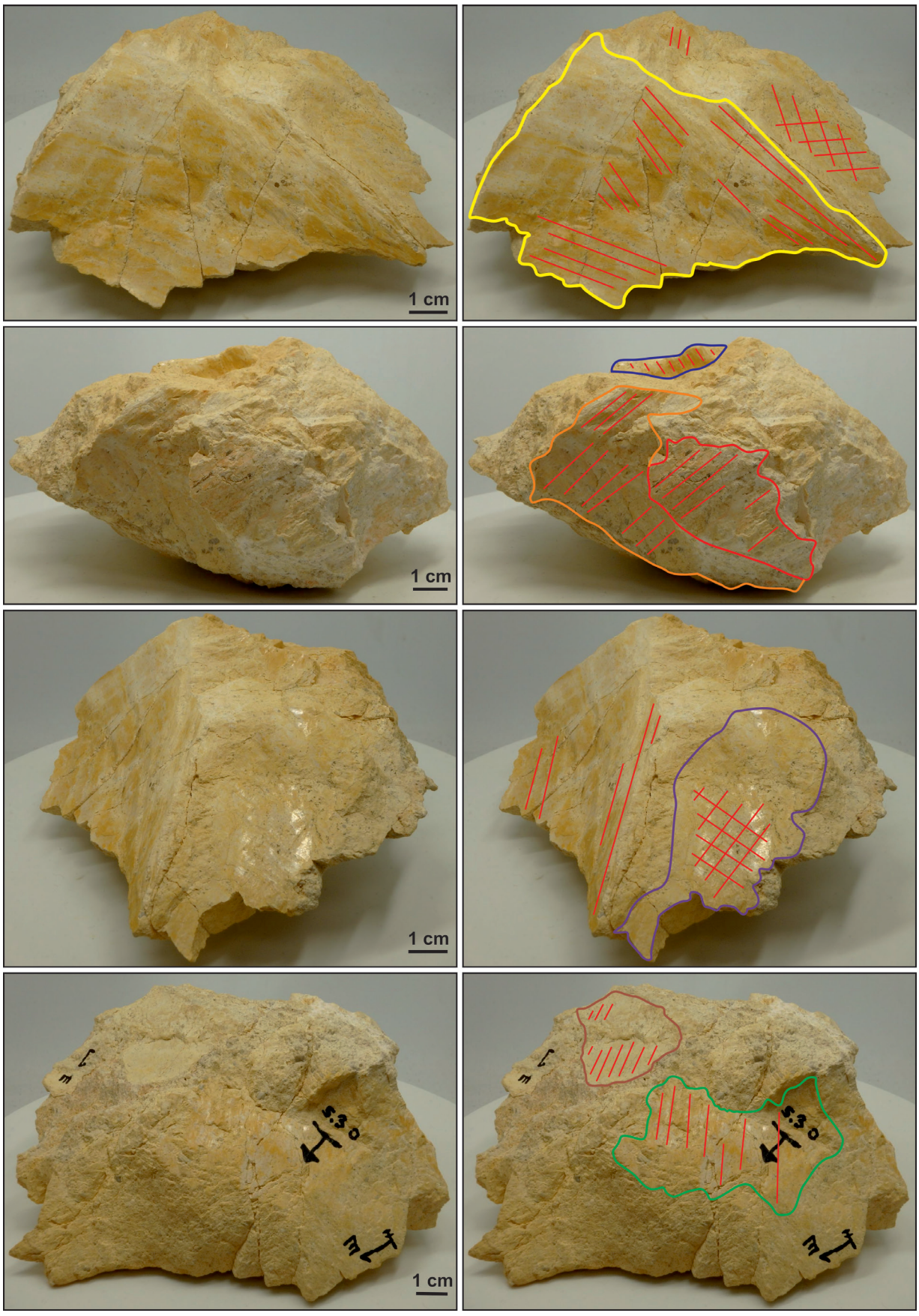

Figure 5: Photographs of the different sides of the hand sample OB5.3. Distinctly polished slickensides are outlined in different colours. Lineation directions are marked in red. Adjacent polished slickensides of different orientation sometimes show deviating lineation directions.

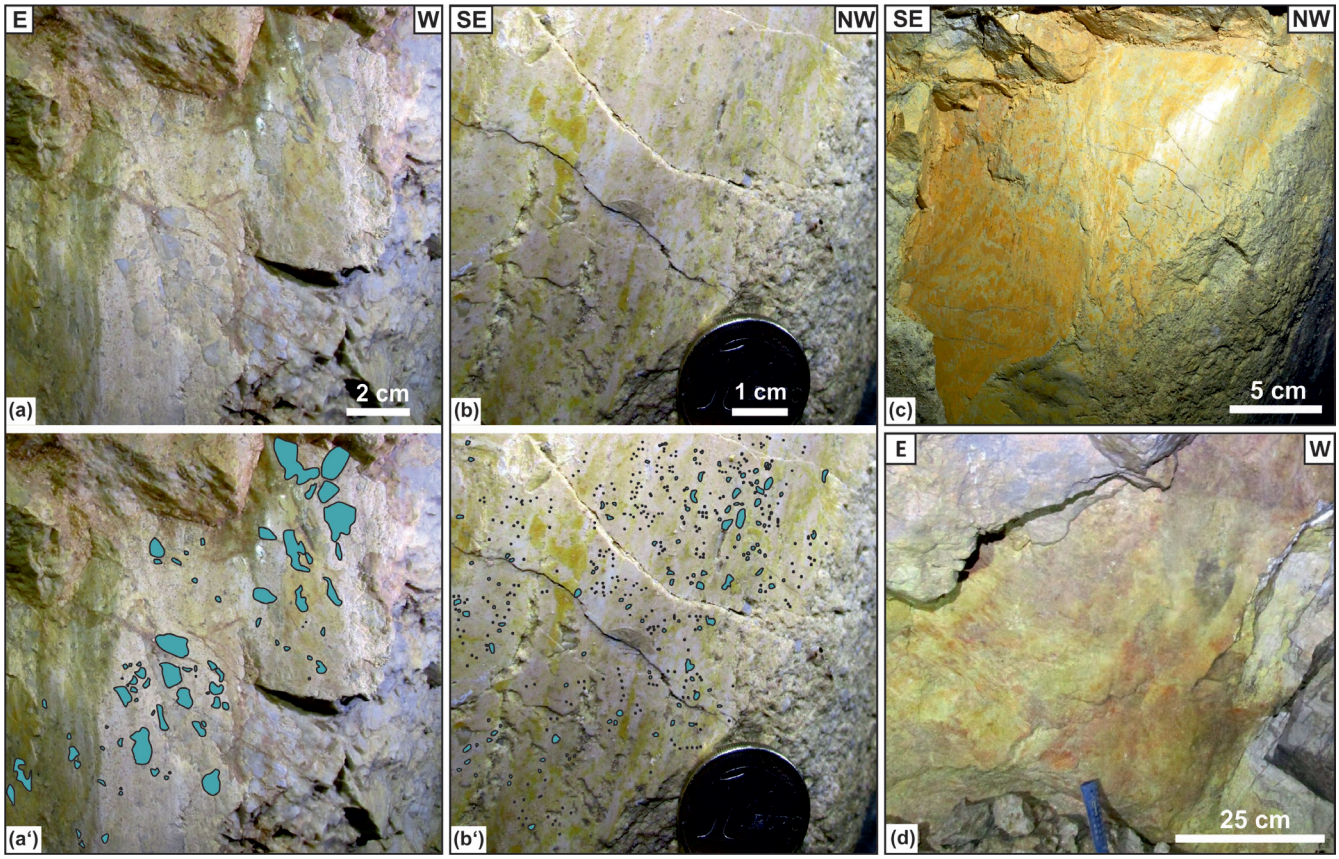

Figure 6: Examples for differences between the individual polished slickensides documented in the Wartburg Cave. They range in size from a few centimetres up to 1 m. For their localisation see Figure 2. **(a)** and **(b)** Truncated grains vary in distribution and size. **(a')** and **(b')** Sizes from 0.25 to 14 mm are delineated in the photographs below. **(c)** and **(d)** Different colours (from white to reddish-brown) of the ultracataclasite can be distinguished on the polished surfaces.

sample, OB10, was collected from polished bedrock and consists almost entirely of undeformed rock. From the transition zone, thin section OB8 gives a good overview of the different cataclastic deformation stages. All other samples were taken from deformed rock. A detailed documentation of all samples is given in Koppensteiner (2021).

4.2.1. Slip surfaces, types of cataclasites and cataclastic maturity

The straight (Fig. 8i) or curved (Fig. 8a) slip surfaces cut through various types of cataclasites, from proto- to ultracataclasite. Depending on the maturity of the cataclasite the clasts appear in sizes from less than 0.1 up to 6 mm. They show different shapes from angular to almost perfectly rounded (Fig. 9). Ultracataclasites with rounded clasts often accumulate directly under the principal slip surface or fill the interstices between fragmented grains or fractures. With the optical microscope it was possible to distinguish minimum grain lengths of 0.01 mm, but these grains are embedded in even more fine-grained material.

To identify the cataclastic maturity of the deformed bedrock, three thin sections were selected according to the polishing grade of the hand samples (intermediate and highly polished slickensides; cf. section 3). Parallel offsets and V-shaped zones of deformation separating the clasts as well as rotations of fragments occur. Some of the remaining grains have straight grain boundaries on one side while they are rounded to subrounded on the other sides.

Sample OB3a (Fig. 9) shows the cataclasites of a slip zone bordered by an irregular slip surface, which cuts several clasts (see section 4.2.2). The up to several millimetres large clasts are separated by a fine-grained matrix, which also fills the gaps between fractured grains. Most of the clasts are subangular but close to the slip surface there is an up to 3 mm thick layer of ultracataclasite with several up to max. 1 mm large, rounded clasts. This sample shows mostly average maturity of the host rock, with the uppermost part just below the mirror surface being more mature. In terms of the stages of cataclastic deformation (see section 3), the deformed rock correlates with stages two and three while stage four occurs only directly beneath the mirror surface with mostly rounded grains. Significant differences in cataclastic deformation were observed in thin section OB8. It shows the evolution from undeformed bedrock to completely comminuted rock fragments embedded in an ultracataclasite (Fig. 7).

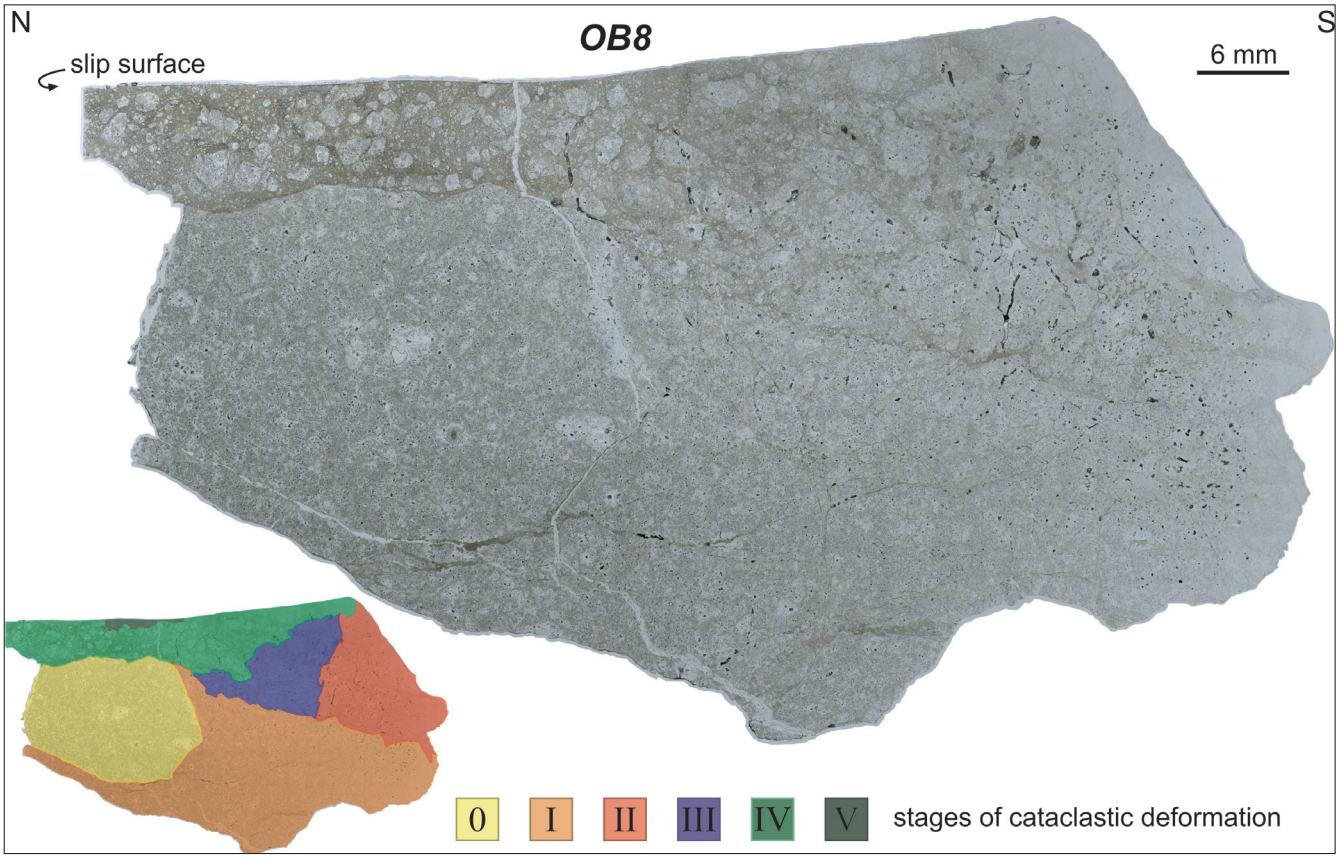

Figure 7: The thin section of the sample OB8 gives a good overview of the different stages of cataclastic deformation from the undeformed bedrock (stage 0) to completely comminuted rock fragments (stage 5).

4.2.2. Truncated grains

In all thin sections, grains of different sizes and shapes are cut by the knife-sharp, polished slip surfaces (Fig. 8a, i). The truncated sides of the grains are either smooth or corrugated depending on the texture of the slip surface that cuts them. Grains are truncated not only by the polished slip surfaces, but also by small fractures.

4.2.3. Clasts

Clasts can originate not only from the bedrock, but also from older cataclasites or vein calcites. These clasts are comminuted by Mode I and Mode II fractures. Fragments of fractured grains can show parallel fracture planes or show a V-shaped zone of deformation between them (Fig. 8c, d). The V-shaped microstructures occur only locally, where adjacent areas and grains show mostly different displacement directions or no evidence of displacement at all.

4.2.4. Fractures and slip surfaces within the slip zone

Fractures cross-cut the ultracataclasite, the bedrock and clasts of the bedrock. They occur in four different variations: open, sealed by ultracataclasite, sealed by blocky calcite crystals or sealed by intensely twinned calcite crystals. Systematic fracture networks crosscut some of the investigated samples, e.g. OB3b, where the ultracataclasite is cut by further slip surfaces at angles similar to R and R', and by other, apparently younger slip surfaces in a third direction (Fig. 10).

4.2.5. Pressure solution seams

Pressure solution seams traverse the ultracataclastic matrix of most of the thin sections. They appear in the form of small areas or along the boundaries of fragmented grains, where they often cover them (Fig. 8i). The pressure solution seams occasionally develop as a SC/SCC' cleavage and can be described as a pressure solution cleavage, which can occur as connecting elements between the steps of a relay (Fig. 11a). It also occurs at high angles to systematic fracture networks that cross-cut the protocataclasite (Fig. 11b, b').

4.2.6. Rhombohedral dolomite crystals

Almost perfectly rhombohedral dolomite crystals occur in several thin sections in different amounts. They appear scattered, cumulated beneath the slip surface, clustered between grains and cumulated in other parts of the thin sections. Bigger crystals are partly broken and show distinct zoning and/or fluid inclusions (Fig. 8e). In veins or at the edges of ultracataclastic injection veins rhombohedral dolomite crystals with distinct zoning and mostly bent grain boundaries occur (Fig. 8f). Brighter

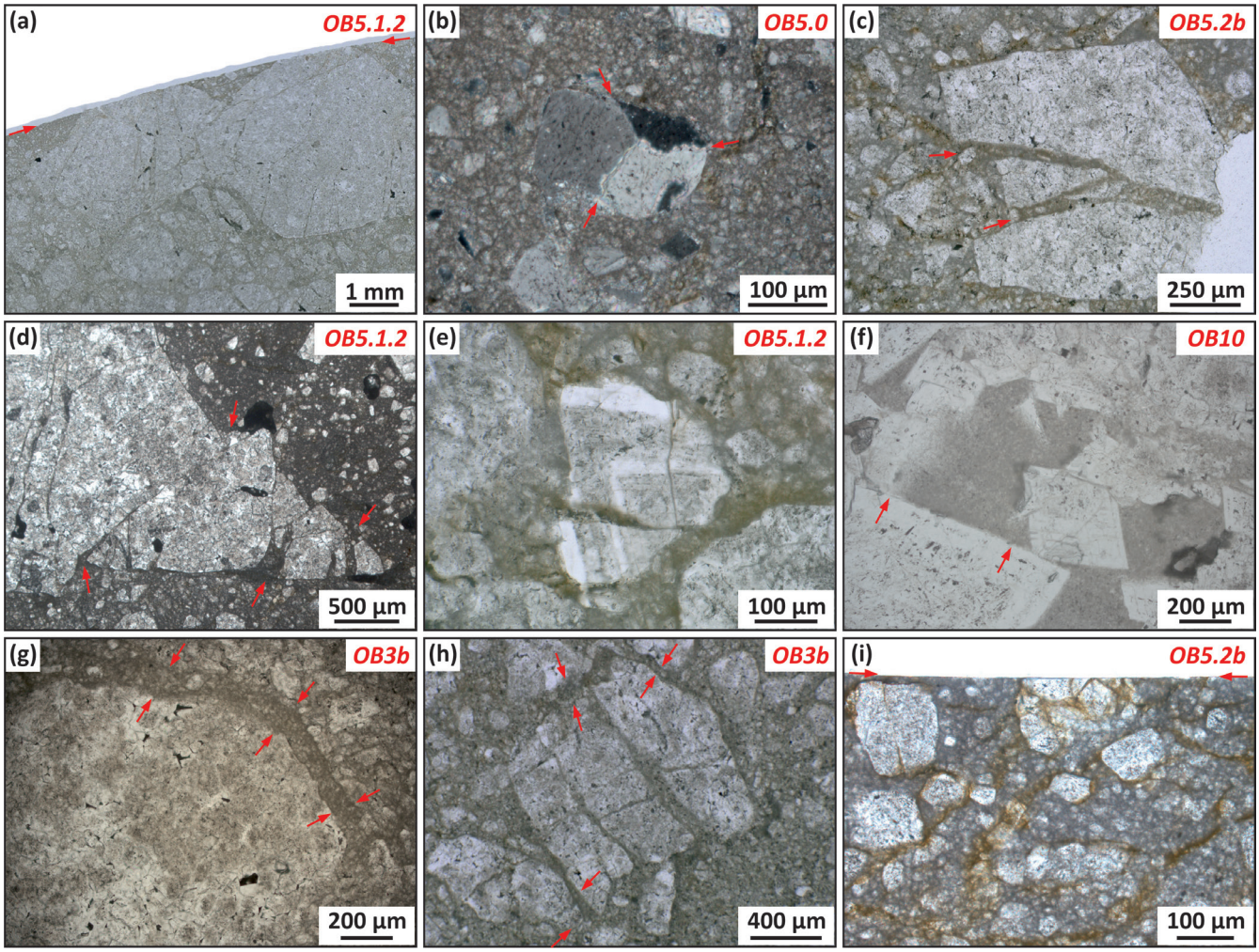

Figure 8: Compilation of the most important features of the thin sections examined under PPL (red arrows indicate the microstructures investigated). **(a)** The partly curved polished slickenside truncates grains. **(b)** Grain in the centre with triple junction (photo taken under cross-polarised light). **(c)** and **(d)** Parallel offsets and V-shaped deformation zones between fragments of grains, which are partly shifted as well. **(e)** Broken fragment of a rhombohedral dolomite crystal with zoning and fluid inclusions. **(f)** Rhombohedral dolomite crystals with surrounding very fine-grained material. The one in the lower left corner shows slightly bent crystal boundaries. **(g)** and **(h)** Injections of ultracataclastic material around grain fragments. **(i)** Pressure solution seams as orange-brown lines traversing the ultracataclasite and accumulating along fractures and around grains. Note the knife-sharp polished slickenside truncating one of the grains.

crystals with less fluid inclusions show angular to subrounded shapes and partly lobate grain boundaries. Triple junctions appear under XPL in many of these crystals (Fig. 8b).

4.2.7. Dilation

Dilation is visible in veins, V-shaped deformation zones and ultracataclastic injections. Injections or injection veins of ultracataclastic material occur in different shapes and extent within almost every thin section (Fig. 8g, h). They surround parts of one grain, several grain fragments or fill up bigger areas. Some of these areas were also observed with the digital microscope, which could resolve minimum grain sizes of 5 µm. These grains are embedded in even more fine-grained ultracataclasite. These processes are fluid-assisted and lead to a volume increase of the fault rock (cf. Schuck et al., 2018). The development of isolated V-shaped deformation structures can only take place under fluidisation. The orientations of the openings of the offsets at hand can therefore not be used as shear-sense indicators as in Hippertt (1993), who worked on feldspar porphyroclasts in granite mylonites at low metamorphic grades.

4.2.8. Surface topography models

The smoothness of the polished surfaces and of the lineations of three highly polished samples were examined using surface topography models (Fig. 12). The investigated fault mirrors are partly corrugated parallel to the striation and show truncated grains of the cataclastic host rocks. The 3D surface topography models revealed a maximum vertical distance of 17 to 62 µm between the highest and lowest surface points. As the profiles had a maximum height difference of 3.5 and 22 µm in the di-

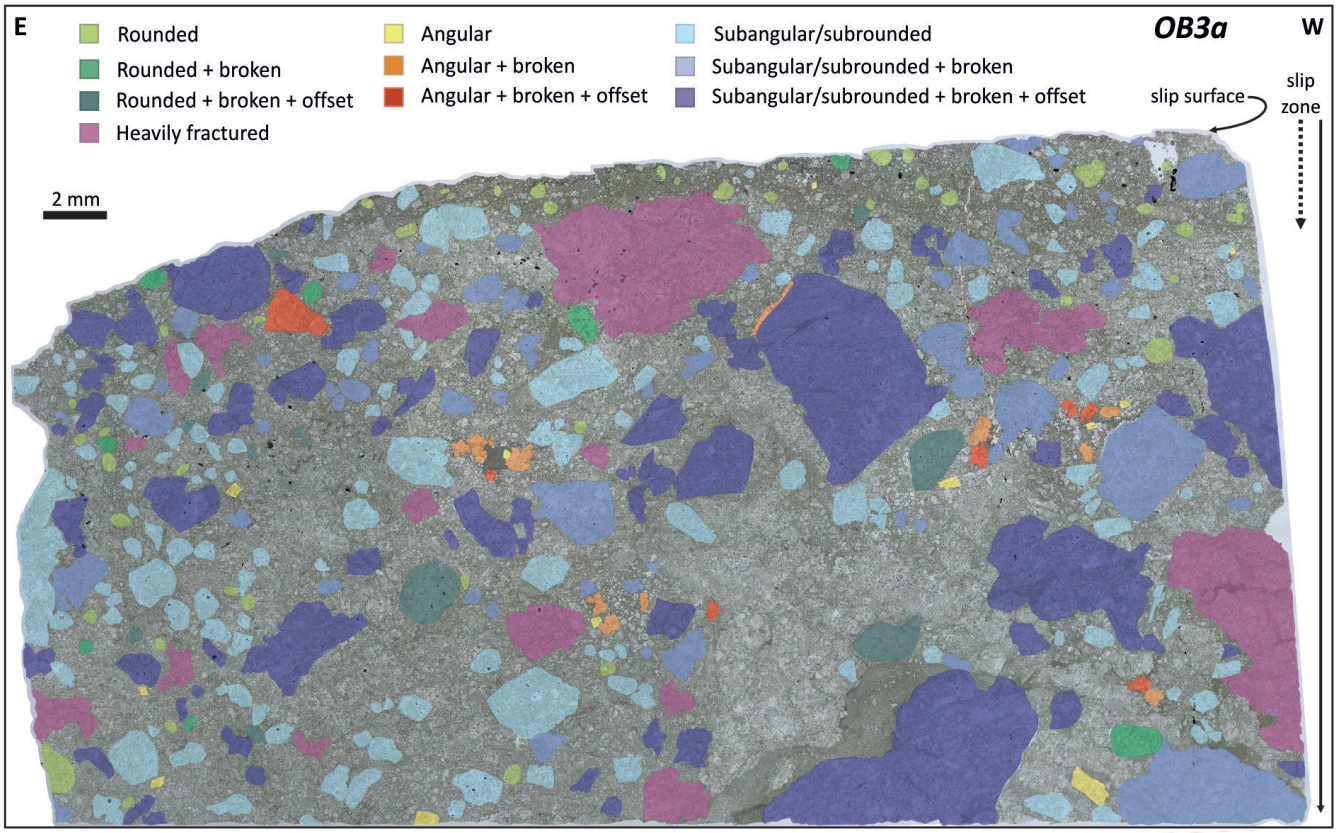

Figure 9: Map of cataclastic maturity of thin section OB3a. Different colours indicate different grains shapes and highlight different degrees of maturity. In areas without coloured grains, the grain sizes were too small to be considered or there were no clear boundaries between grains. Subangular/subrounded grains are the most common and most evenly distributed. The dotted arrow of the slip zone indicates the area directly beneath the slip surface, which is mostly composed of ultracataclasite and rounded grains.

rection of the lineation, the striae can be described as completely polished.

4.3. Mineral composition

An XRD analysis was conducted on material from a sample containing numerous truncated grains smaller 1 mm^2 appearing along mirror surfaces with polishing grades of 5. The results showed that dolomite is the main component, and calcite occurs only in traces.

5. Interpretation and discussion

5.1. Relation of the investigated outcrops to the Obir Fault

Fault planes measured in the Wartburg Cave and at the surface show a wide range of dips, with clusters of steeply dipping planes in SE and NW directions, respectively. Thus, the mean strike in NE-SW direction (Fig. 4) fits the main ENE-WSW orientation of the Obir Fault as described in Baroň et al. (2019b). All faults have moderately steep to steep dip angles and no (sub-) horizontal fault surfaces were observed. This pattern correlates with a strike-slip fault system with secondary faults in a damage zone (Sylvester, 1988; Wilcox et al., 1973; Woodcock and Schubert, 1994; Fossen, 2016).

The polished slickensides at the investigated exposure in the Wartburg Cave occur within a wall section of about 10 m in length, directly adjacent to two main fault planes striking across the cave. The ones found near the entrance of the mining tunnel directly above the "Markusstollen" were also located around a main fault surface. No other occurrences of polished slickensides were found nearby inside the cave and the mining tunnels. Thus, the proximity of the polished slickensides to main fault planes seems essential for their formation.

Schröckenfuchs et al. (2015) studied a strike-slip fault zone in dolomite rocks and showed that mirror slickensides occur commonly in cataclastic slip zones. They are located within fractured wall-rock as well as in transition of damage zones and fault cores. The striated mirror slickensides observed in this study occur in three different forms: directly in the bedrock, mostly covered by polished cataclastic material or in cataclastic slip zones (samples of exposure OB5). We suggest that the formation of the polished slickensides found on the surface and underground in the area of the Untere Schäfleralm is related to movements of the Obir Fault and that the surface outcrops and sub-surface exposures with the polished slickensides are the damage zones or fault cores of minor fault zones within the Obir Fault System.

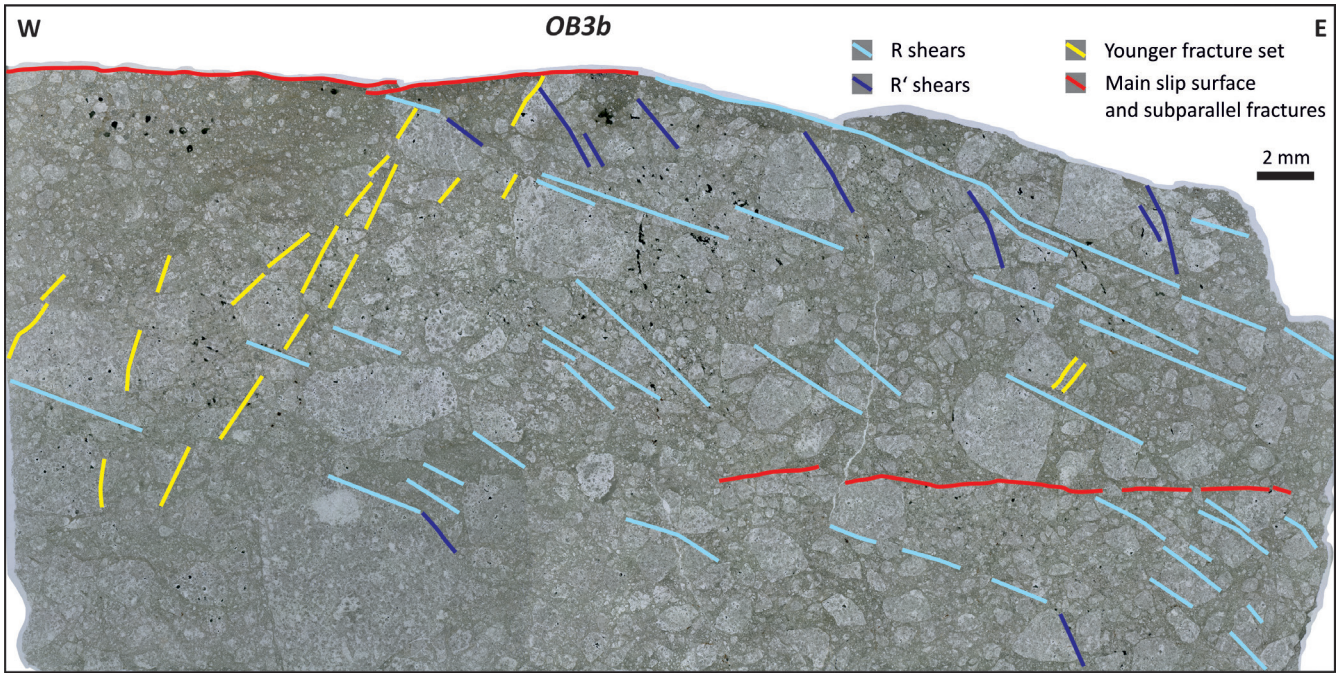

Figure 10: Secondary faults marked in a stitched high-resolution photomicrograph of OB3b, taken under plane-polarised light. Different colours were used: 39 R-fractures (light blue) and 10 R'-fractures (dark blue) indicating dextral shear sense, 21 younger fractures (yellow) and seven fractures sub-parallel to the polished slickenside. Although not visible in the matrix, the fractures are assumed to continue through the thin section and into the adjacent rock.

5.2. Is the Obir Fault seismically active?

The investigated fault rocks show alternating episodes of dilation, slip, cataclasis and sealing processes, indicating that the rock has undergone periods of different rheological behaviour. Examples are the synthetic and antithetic Riedel fault surfaces, which are the only reliable indicators of the different shear senses identified in this study (Fig. 10). In contrast, the absence of strain shadows within the ultracataclasite next to rotated clasts, parallel offsets or V-shaped deformation zones between grain fragments is only possible if the rock has been fluidised allowing the matrix to behave like a suspension. The presence of rounded grains next to angular ones as well as the re-fracturing of rounded grains shows the different degrees of deformational maturity of the rock. To achieve such diversity, several events of cataclastic comminution are necessary. Some observations from this study are then discussed in terms of their implications for the above question.

5.2.1. Polished slickensides

The polished surfaces presented are characterized by pervasive areas of a few square centimetres in size, partly irregular, with different orientations and lineations (Fig. 5) and offset in the order of a millimetre. The diversity of so many centimetres-sized and polished slickensides occurring in such a confined area close to a major fault is not consistent with tens of meters large fault mirrors (Siman-Tov et al., 2013) or with displacements in rotary shear experiments in the order of tens of centimetres to metres (Siman-Tov et al., 2015).

5.2.2. Cataclasis and cataclastic flow

Cataclasis and cataclastic flow are the main deformation processes, in which grain fragmentation subsequently causes compaction and rearrangement (sliding and rotation) of the new fragments within the pre-existing pore space (Sibson, 1977; Evans, 1988; Blenkinsop 1991; Rutter and Hadizadeh, 1991; Lin, 2001; Passchier and Trouw, 2005). This leads to strain hardening, which is typical of the cataclastic flow regime (Renner and Rummel, 1996; Kenkmann, 2003; Kohlmayer and Grasemann, 2012). During cataclasis further fracturing and crushing of grains is coupled with frictional sliding that can occur along grain boundaries (Fossen, 2016). Power and Tullis (1989) investigated cataclastically deformed principal slip zones and suggested that the cataclasis occurred at high strain rates during seismic slip.

5.2.3. Truncated grains

Along the slip surfaces many grains are truncated knife-sharp without any further signs of deformation like fracturing or twinning. This is typical of principal slip surfaces and polished fault surfaces, which are attributed to seismic slip (Fondriest et al., 2013; Siman-Tov et al., 2013; Verberne et al., 2014; Kuo et al., 2016). The truncated grains along highly polished principal slip surfaces as well as fluidised ultracataclasites are comparable to potential seismic markers, which were described in other fault zones (Demurtas et al., 2016; Tschegg et al., 2020; Ferraro et al., 2018; Vignaroli et al., 2020).

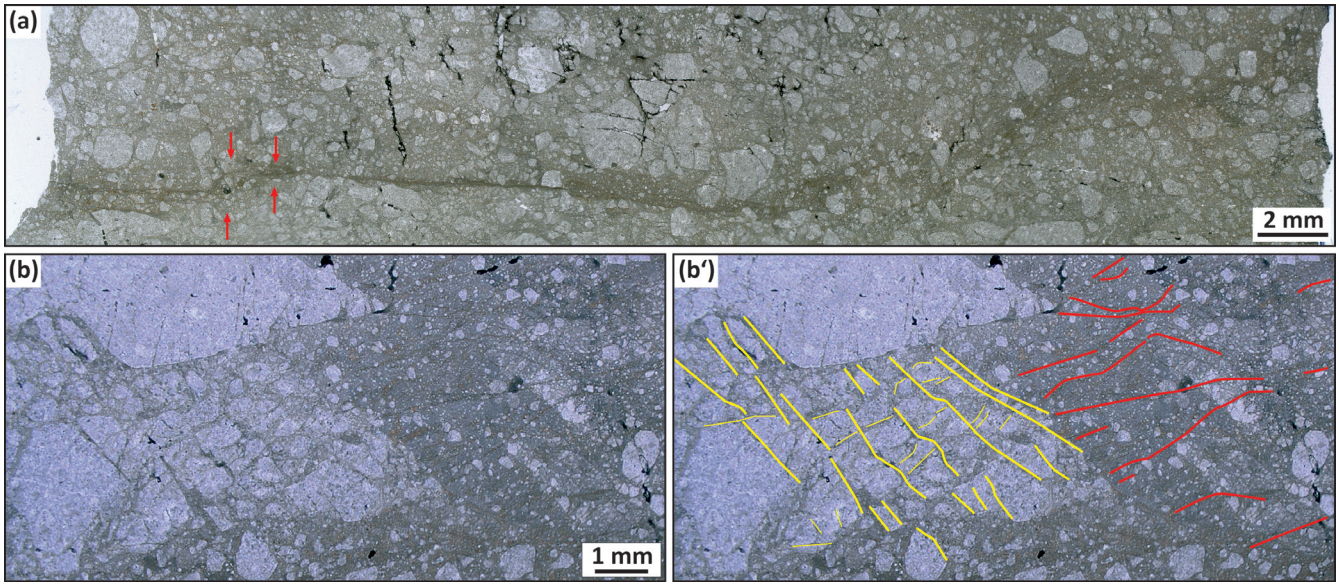

Figure 11: Photomicrographs highlighting the characteristics of ultracataclastic fluidisation, pressure solution seams and illuviated calcite crystals of the principal slip zones associated to the Obir Fault. **(a)** SC/SCC′ cleavages of pressure solution seams as steps in a relay marked with red arrows in thin section OB5.1.1. **(b)** and **(b')** Cataclastically heterogeneous slip zone in thin section OB5.1.2. The protocataclasite of the slip zone is cross-cut by systematic fracture networks (marked in yellow) while the cataclasite is traversed by pressure solution seams (marked in red) at high angles to the dominant fracture set.

5.2.4. Calcite crystals

Larger calcite crystals with partly lobate grain boundaries and only few fluid inclusions occur in about half of the investigated thin sections. Several crystals show not only undulose extinction under XPL but also triple junctions (Fig. 8b). A large number of these crystals occur in thin section OB5.0. Due to their occurrence in the partly flowstone covered exposure, they are interpreted as fragments of speleothems, which were transported into the rock during a fluid-rich phase of co-seismic deformation. Similar findings were reported from Baqués et al., (2011), who worked on cataclasites of carbonate precipitations within fractures that were affected by multiple episodes of fracturing during faulting. Sanders et al. (2018), Szczygieł et al. (2021), Sala et al. (2022) and Mitrović-Woodel et al. (2023) also investigated speleothem flowstones containing evidence of intermittent fracturing, which were interpreted from episodic downfaulting or co-seismic shaking during speleothem growth and concluded as a presumably result of co-seismic deformation.

5.2.5. Dilation

In many of the investigated thin sections dilation is recorded in the form of injected fault rock, which appears as seams around grains, irregularly shaped ultrafine-grained areas or V-shaped deformation zones (Fig. 8). Fluidised fault rocks are commonly associated with injections or protrusions of fault rock material from one rock part into another. Fluidised cataclasites and injections of clastic fault rock are suggested to be a useful indicator for seismic slip (Brodsky et al., 2009; Otsuki et al., 2003; Smith et al., 2008, 2011; Ujiie et al., 2007; Lin, 2011; Rowe et al., 2005, 2012).

5.2.6. Ultracataclasite and pulverised rocks

The high abundance of ultracataclasite and ultrafine-grained matrix in the samples investigated reminds of pulverised rocks, which, usually observed in quartzo-feldspathic rocks, are a distinct type of fault rock. They have been linked to co-seismic damage and were found near major strike-slip faults like the San Andreas Fault System in California (Dor et al., 2006; Brune et al., 2001; Rempe et al., 2013). The grain size of these pulverised rocks is <1 mm on average. Their original texture (e.g., grain boundaries and foliation surfaces) is preserved as they do not show evidence of (1) significant shear strain at the macro- and microscale, (2) grain rotation and (3) rounding (Dor et al., 2006; Wechsler et al., 2011; Schröckenfuchs et al., 2015; La Valle et al., 2019).

Records of pulverised rocks in carbonates are rare. They were first recognised in the Italian Southern Alps and Central Appennines by Agosta et al. (2006), Fondriest et al. (2012), Fondriest et al. (2015) and Demurtas et al. (2016). Sagy et al. (2012) investigated faults on the Israeli coastal plain and reported pulverised carbonate rocks in drill cores from a depth of 4980–5911 m. Schröckenfuchs et al. (2015) worked on pulverised rocks in dolomites from minor fault branches of the Salzach-Ennstal-Mariazell-Puchberg (SEMP) fault system in the Eastern Alps. Fondriest et al. (2015) described in situ shattered rocks in dolostones as fault breccias with exploded jigsaw textures and preserved original sedimentary fabric at an average grain size of <1 mm. Baroň et al. (2022a) documented such rocks NE of the Obir Caves, which are described in this study as screes of shattered carbonate rocks. The high grade of pulverisation observed in the samples of

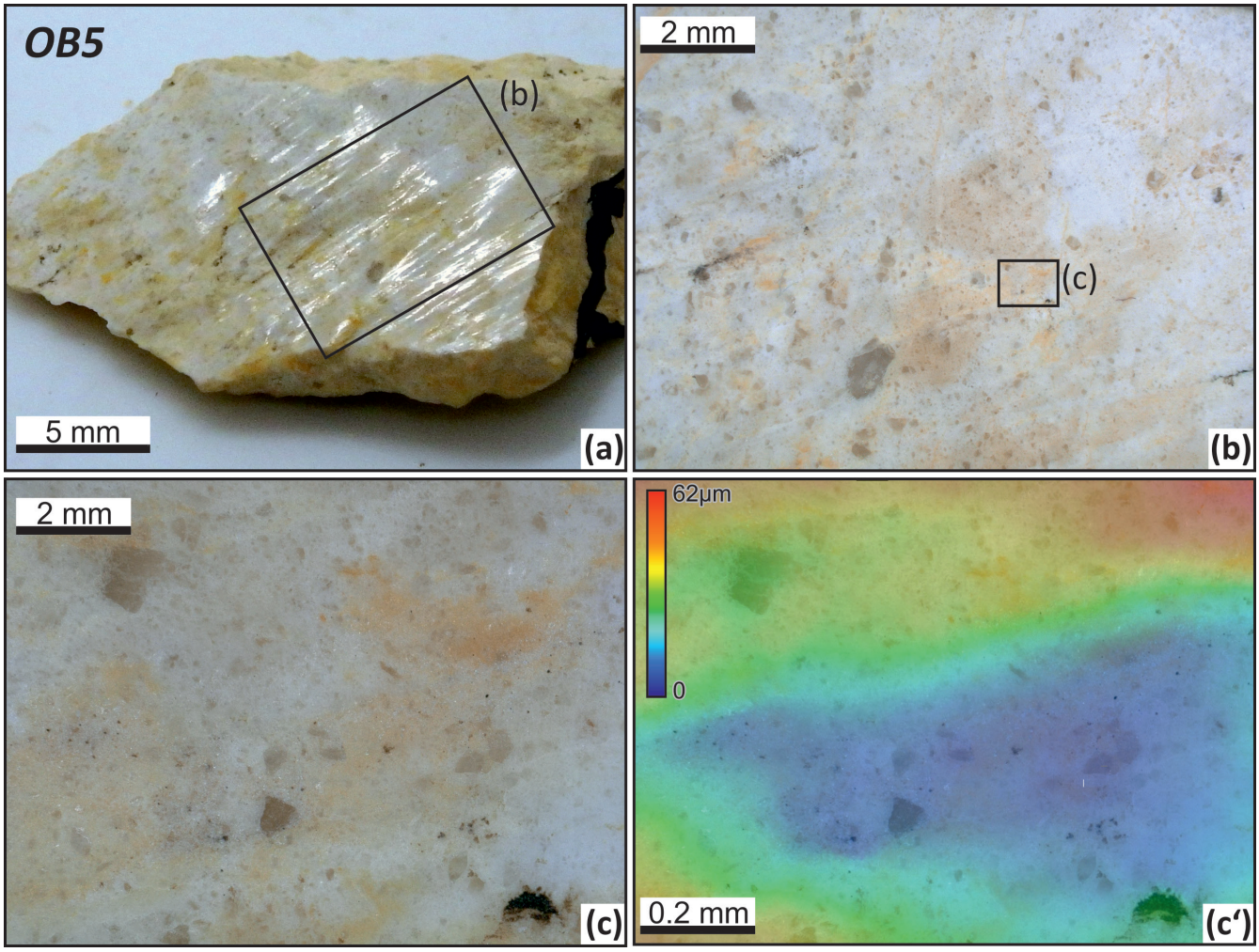

Figure 12: Investigation of the roughness of the polished slickenside of sample OB5. **(a)** Photograph of polished slickenside. **(b) (c)** Different magnifications of the area of interest. **(c')** Surface topography model from 141 images taken with a step size of 0.5 µm. Same area as pictured in **(c)**.

polished slickensides from this study is interpreted as another indicator for seismic slip (cf. Payne and Duan, 2016).

5.2.7. Pressure solution seams

Pressure solution seams and cleavages are a result of fluid-assisted intergranular pressure solution (IPS), which involves stress-driven dissolution of material along grain contacts (Rutter, 1976; Rutter, 1983; Renard et al., 2000; Gratier and Gueydan, 2007; Zhang et al., 2010; Smith et al., 2011; Nenna and Aydin, 2011). IPS is common in carbonate rocks, which have experienced low-grade metamorphic and diagenetic conditions (Tada and Siever, 1989; Billi, 2010; Billi, 2003; Renard et al., 2004; Smith et al., 2011). Zhang et al. (2010) conducted uniaxial compaction experiments on wet calcite aggregates at post-seismic strain rates. Their results suggest that IPS is a typical deformation mechanism in natural principal slip zones during shallow post-seismic slip/post-seismic stress relaxation in carbonate rocks within and surrounding a fault zone (Renard et al., 2004; Gratier et al., 2003; Gratier and Gueydan, 2007; Smith et al., 2011). Based on the location of the exposure within the Obir Fault and the results of Baroň et al. (2019b), who recorded aseismic movements directly adjacent to it, the formation of the pressure solution structures is assumed to be aseismic during post-seismic slip.

5.2.8. Recent fault acitivity

Recent movements of the Obir Fault are evident in the many broken speleothems in the individual sections of the Obir Caves (Baroň et al., 2022a). On-going movements are recorded in the Wartburg Cave with two monitoring TM71 devices (Baroň et al., 2019a, 2019b). These studies show that the Obir Fault has not only been active in the past, but is still an active fault today.

5.3. Conceptual model on the formation of the fault mirrors

The polished slickensides investigated, which exhibit various spatial orientations, are found exclusively close to the Obir Fault. Since these faults are only a few centimetres long, they have recorded displacements on the

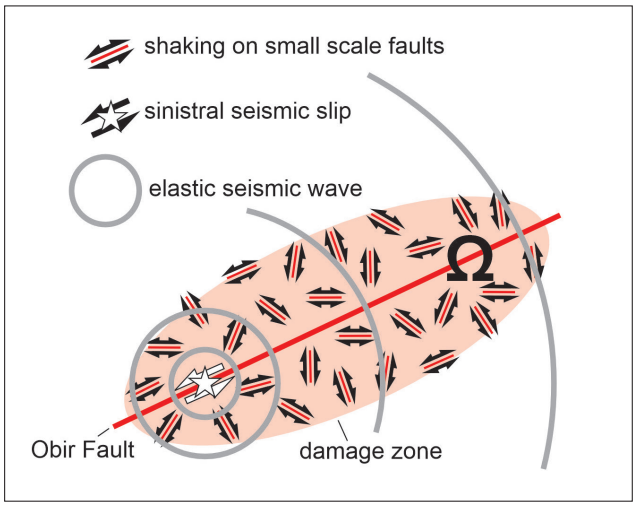

Figure 13: Conceptual model on the formation of fault mirrors. Seismic slip on a patch of the Obir Fault releases elastic seismic waves causing shaking on small scale faults in the damage zone. The shaking results in smoothing and eventually polishing of the small slip surfaces. The omega symbolises the location of the cave.

order of millimetres. This limited displacement cannot account for the polished fault surfaces, regardless of whether the slip was seismic or aseismic (Fondriest et al., 2013; Siman-Tov et al., 2013; Verberne et al., 2013; Tesei et al., 2017). We therefore propose an alternative conceptual model to explain the near-surface polishing of faults with minimal size and displacement (Fig. 13). The Obir Caves are situated directly north of the core of the W-E trending Periadriatic Fault in the Northern Karawanks, an area known for fault activity since the Miocene (Ratschbacher et al., 1991; Fodor et al., 1998; Vrabec et al., 2006). Displacement along the Obir Fault or another nearby fault could have released energy in the form of body or surface seismic waves, causing near-surface shaking. Such shaking could have induced elastic deformation and minor back-and-forth motion along the small-scale faults in the damage zone of the Obir Fault. Since the polished slip surfaces show no evidence of healing by fluid precipitation, it is plausible that multiple shaking events contributed to their smoothing and polishing. It is important to note that millimetre-scale motion would be associated with very short wavelengths and, consequently, high frequencies, which are only observed in close proximity to the epicentre due to attenuation. We therefore propose that small-scale fault mirrors can serve as indicators of a short distance (< several kilometres) from the epicentre.

Although more detailed studies, including experiments, are needed in the future, such a scenario would explain (i) polishing of surfaces measuring (some) square centimetres, (ii) polishing of irregular surfaces, (iii) neither a preferred orientation of the surfaces nor a dominant set of lineations consistent with the kinematics of the fault, (iv) no visible offset along the slip surfaces, (v) occurrence of swarms of small fault surfaces confined to the vicinity of large scale faults.

6. Conclusions

This study focused on the detailed investigation of polished slickensides, which formed along a segment of the Obir Fault in the Northern Karawanks (Carinthia, Austria). Slip zones of the Obir Fault System cut carbonate bedrock within the Wartburg Cave (part of the Obir Caves) and in the surrounding area on the surface. Spatial measurements of slickensides from inside and outside the Wartburg Cave fit well with the main ENE-SWS direction of the Obir Fault. Fieldwork revealed only steep and medium-steep fault surfaces, while flat ones were missing.

The slip zones of secondary faults contain protocataclastic and cataclastic fault rocks and are delimited by a polished, mirror-like slip surface. These striated polished slickensides can be straight or curved and occur directly on the bedrock, mostly covered by polished and cataclastically deformed bedrock or in cataclastic slip zones. The polishing grade of the slip surfaces found outside the cave is generally lower compared to the ones found in the Wartburg Cave.

Microstructural investigations revealed different stages of cataclastic deformation within the samples taken from Wartburg Cave. Systematic fracture networks crosscut some samples, while the ultracataclastic matrix of most samples is traversed by pressure solution structures. Fluidisation occurring as ultracataclastic injections between clasts and ultracataclasite suggests protrusion of material from the surrounding rock.

The microstructures, including polished slickensides, injected cataclasites and truncated grains along principal slip surfaces, together with the geological position close to the seismogenic Periadriatic Fault System and the nearby screes of shattered carbonate rocks on the surface suggest that the investigated fault surfaces in the Obir Caves were formed during seismic slip. In contrast, the presence of pressure solution cleavages indicates periods of aseismic deformation.

We propose a conceptual model in which rock segments form between the main and secondary faults (Fig. 13). The high angles between these faults and the absence of flat fault surfaces lead to the jamming or wedging of these rock segments. Then small-scale shaking movements during a seismic wave causes the development of minor faults with small polished slickensides.

Acknowledgements

We are thankful to the operators and landowners of the Obir Caves for allowing us to take the samples in the Wartburg Cave. Fruitful discussions are appreciated with S. Klackl, M. Werdenich, A. Schagerl, M.S. Hollinetz and E. Draganits. We would also like to thank Z. Hou for his support while working on the digital microscope. Further thanks for discussions and help go to H. Rice, U. Klötzli, P. Meister, M. Moser, M.J. Coleman and Su. Gier. IB acknowledges the long-term conceptual development research organisation RVO: 67985891 at the Institute of Rock Structure and Mechanics of the Czech Academy of Sciences

in Prague and the SPELEOTECT project P25884-N29 financed by the Austrian Science Foundation (FWF). Ernst Willingshofer and an anonymous reviewer are acknowledged for their effort and help in improving the quality of the manuscript.

References

Agosta F., Aydin A., 2006. Architecture and deformation mechanism of a basin-bounding normal fault in Mesozoic platform carbonates, central Italy. Journal of Structural Geology, 28/8, 1445–1467. https://doi.org/10.1016/j.jsg.2006.04.006

Baqués V., Travé A., Labaume P., Benedicto A., Soliva R., 2011. Differences between pre-rift and syn-rift karsts in a major Neogene normal fault zone from petrological and geochemical analysis of their infillings. Documentos sobre el Terciario de Iberia a inicios del Siglo XXI, VII Congreso del Grupo Español del Terciario.

Baroň I., Plan L., Sokol L., Grasemann B., Melichar R., Mitrovic I., Stemberk J., 2019a. Present-day kinematic behaviour of active faults in the Eastern Alps. Tectonophysics, 752, 1–23. https://doi.org/10.1016/j.tecto.2018.12.024

Baroň I., Sokol L., Melichar R., Plan L., 2019b. Gravitational and tectonic stress states within a deep-seated gravitational slope deformation near the seismogenic Periadriatic Line fault. Engineering Geology, 261. https://doi.org/10.1016/j.enggeo.2019.105284

Baroň I., Plan L., Grasemann B., Melichar R., Mitrović-Woodell I., Rowberry M., Scholz D., 2022a: Three large prehistoric earthquakes in the Eastern Alps evidenced by cave rupture and speleothem damage. Geomorphology, Volume 408. https://doi.org/10.1016/j.geomorph.2022.108242

Baroň I., Koktavý P., Trčka T., Rowberry M., Stemberk J., Balek J., Plan L., Melichar R., Diendorfer G., Macků, R., Škarvada, P., 2022b. Differentiating between artificial and natural sources of electromagnetic radiation at a seismogenic fault. Engineering Geology, 311, 106912. https://doi.org/10.1016/j.enggeo.2022.106912

Bauer F. K., Schermann O., 1984. Das Periadriatische Lineament in den Karawanken. Jahrbuch der Geologischen Bundesanstalt, Wien, 127, 299–305. https://opac.geologie.ac.at/ais312/dokumente/JB1273_299_A.pdf

Billi A., 2003. Solution slip and separations on strike-slip fault zones: theory and application to the Mattinata Fault, Italy. Journal of Structural Geology, 25, 703–715. https://doi.org/10.1016/S0191-8141(02)00077-9

Billi A., Toro G.D., 2008. Fault-related carbonate rocks and earthquake indicators: recent advances and future trends. In Landowe, S. J. and Hammler, G. M., editors, Structural Geology: New Research, 63–86. Nova Science Publishers, Inc.

Billi A., 2010. Microtectonics of low-P low-T carbonate fault rocks. Journal of Structural Geology, 32, 1392–1402. https://doi.org/10.1016/j.jsg.2009.05.007

Blenkinsop T.G., 1991. Cataclasis and processes of particle size reduction. Pure and Applied Geophysics PAGEOPH, 136, 59–86. https://doi.org/10.1007/BF00878888

Bögel H., 1975. Zur Literatur über die „Periadriatische Naht". Verhandlungen der Geologischen Bundesanstalt, Wien, 2, 163–199.

Brodsky E.E., Rowe C.D., Meneghini F., Moore J.C., 2009. A geological fingerprint of low-viscosity fault fluids mobilized during an earthquake. Journal of Geophysical Research: Solid Earth, 114. https://doi.org/10.1029/2008JB005633

Brune J.N., 2001. Fault-normal dynamic unloading and loading: An explanation for "Non-Gouge" rock powder and lack of fault-parallel shear bands along the San Andreas Fault. AGU, Fall Meeting Supplement, 82/47, F854.

Clar E., 1953. Zur Einfügung der Hohen Tauern in den Ostalpenbau. Verhandlungen der Geologischen Bundesanstalt, Wien, 2, 93–104. https://opac.geologie.ac.at/wwwopacx/wwwopac.ashx?command=getcontent&server=images&value=VH1953_093_A.pdf

Demurtas M., Fondriest M., Balsamo F., Clemenzi L., Storti F., Bistacchi A., Toro G.D., 2016. Structure of a normal seismogenic fault zone in carbonates: The Vado di Corno Fault, Campo Imperatore, Central Apennines (Italy). Journal of Structural Geology, 90, 185–206. https://doi.org/10.1016/j.jsg.2016.08.004

Dor O., Ben-Zion Y., Rockwell T.K., Brune J., 2006. Pulverized rocks in the Mojave section of the San Andreas Fault Zone. Earth and Planetary Science Letters, 245/3–4, 642–654. https://doi.org/10.1016/j.epsl.2006.03.034

Evans J.P., 1988. Deformation mechanisms in granitic rocks at shallow crustal levels. Journal of Structural Geology, 10, 437–443. https://doi.org/10.1016/0191-8141(88)90031-4

Ferraro F., Grieco D.S., Agosta F., Prosser G., 2018. Space-time evolution of cataclasis in carbonate fault zones. Journal of Structural Geology, 110, 45–64. https://doi.org/10.1016/j.jsg.2018.02.007

Fodor L., Jelen B., Márton E., Skaberne D., Čar J., Vrabec M., 1998. Miocene-Pliocene tectonic evolution of the Slovenian Periadriatic fault: Implications for Alpine-Carpathian extrusion models. Tectonics, 17, 690–709. https://doi.org/10.1029/98tc01605

Fondriest M., Smith S.A., Toro G.D., Zampieri D., Mittempergher S., 2012. Fault zone structure and seismic slip localization in dolostones, an example from the Southern Alps, Italy. Journal of Structural Geology, 45, 52–67. https://doi.org/10.1016/j.jsg.2012.06.014

Fondriest, M., Smith, S. A. F., Candela, T., Nielsen, S. B., Mair, K., and Toro, G. D., 2013. Mirror-like faults and power dissipation during earthquakes. Geology, 41, 1175–1178. https://doi.org/10.1130/G34641.1

Fondriest M., Aretusini S., Toro G.D., Smith S.A., 2015. Fracturing and rock pulverization along an exhumed seismogenic fault zone in dolostones: The Foiana Fault Zone (Southern Alps, Italy). Tectonophysics, 654, 56–74. https://doi.org/10.1016/j.tecto.2015.04.015

Fossen H., 2016. Structural Geology. Cambridge University Press, United Kingdom, 2nd edition. https://doi.org/10.1017/9781107415096

Frisch W., Kuhlemann J., Dunkl I., Brügel A., 1998. Palinspastic reconstruction and topographic evolution of the Eastern Alps during late Tertiary tectonic extrusion. Tectonophysics, 297. https://doi.org/10.1016/S0040-1951(98)00160-7

Froitzheim N., Plasienka D., Schuster R., 2008. Alpine tectonics of the Alps and Western Carpathians. In The geology of Central Europe Volume 2: Mesozoic and Cenozoic, volume 2. The Geological Society of London, London. https://doi.org/10.1144/CEV2P.6

Gratier J.P., Favreau P., Renard F., 2003. Modeling fluid transfer along California faults when integrating pressure solution crack sealing and compaction processes. Journal of Geophysical Research: Solid Earth, 108. https://doi.org/10.1029/2001JB000380

Gratier J.P., Gueydan F., 2007. Deformation in the presence of fluids and mineral reactions: Effect of fracturing and fluid-rock interaction on seismic cycles. In Handy, M.R., Hirth G., Hovius N., editors, Tectonic faults: Agents of change on a dynamic Earth, 319–356. The MIT Press, Cambridge.

Han R., Hirose T., 2012. Clay-clast aggregates in fault gouge: An unequivocal indicator of seismic faulting at shallow depths? Journal of Structural Geology, 43, 92–99. https://doi.org/10.1016/j.jsg.2012.07.008

Hippertt J.F.M., 1993. 'V'-pull-apart microstructures: a new shear-sense indicator. Journal of Structural Geology, 15, 1393–1403. https://doi.org/10.1016/0191-8141(93)90001-Q

Jahne L., 1929. Geschichtliche Entwicklung der Bergbauten am Hochobir. Montanistische Rundschau, 21, 53–60.

Kenkmann T., 2003. Dike formation, cataclastic flow, and rock fluidization during impact cratering: an example from the Upheaval Dome structure, Utah. Earth and Planetary Science Letters, 214, 43–58. https://doi.org/10.1016/S0012-821X(03)00359-5

Kober L., 1955. Bau und Entstehung der Alpen. Deuticke, Wien, 2nd edition.

Kohlmayer N., Grasemann B., 2012. Quantitative characterisation of cataclasites using a statistical approach (analysis of variance). Austrian Journal of Earth Science, Vienna, 105/3,48–60. https://www.ajes.at/images/AJES/archive/Band%20105_3/kohlmayer_grasemann_ajes_105_3.pdf

Koppensteiner S.J., 2021. Polished slickensides preserved in the Obir Caves (Austria) close to the Periadriatic Fault System. Master's The-

sis, University of Vienna, Austria, 221 pp. https://phaidra.univie.ac.at/download/o:1399461

Krainer K., 1998. Mineralbildungen und Lagerstätten des Obir (Exkursion E3). Mitteilungen der Österreichischen Mineralogischen Gesellschaft, Wien, 143, 411–424. https://opac.geologie.ac.at/ais312/dokumente/Mitt_OEMinGes_143_411–424.pdf

Kuo L.-W., Song S.-R., Suppe J., Yeh E.-C., 2016. Fault mirrors in seismically active fault zones: A fossil of small earthquakes at shallow depths. Geophysical Research Letters, 43, 1950–1959. https://doi.org/10.1002/2015GL066882

La Valle F., 2019. Factors controlling the thickness of fault damage zones in carbonates (Central Apennines, Italy). Master's thesis, Università degli studi di Padova, Padova.

Laubscher H.P., 1973. Alpen und Plattentektonik. Das Problem der Bewegungsdiffusion an kompressiven Plattengrenzen. Zeitschrift der Deutschen Geologischen Gesellschaft, 124. https://doi.org/10.1127/zdgg/124/1973/295

Lin A., 2001. S-C fabrics developed in cataclastic rocks from the Nojima fault zone, Japan and their implications for tectonic history. Journal of Structural Geology, 23, 1167–1178. https://doi.org/10.1016/S0191-8141(00)00171-1

Lin A., 2011. Seismic slip recorded by fluidized ultracataclastic veins formed in a coseismic shear zone during the 2008 Mw 7.9 Wenchuan earthquake. Geology, 39, 547–550. https://doi.org/10.1130/G32065.1

Loucks R.G., 1999. Paleocave carbonate reservoirs: Origins, burial-depth modifications, spacial complexity, and reservoir implications. AAPG Bulletin, 83, 1795–1834. https://doi.org/10.1306/E4FD426F-1732-11D7-8645000102C1865D

Mancktelow N.S., Stöckli D.F., Grollimund B., Müller W., Fügenschuh B., Viola G., Seward D., Villa I.M., 2001. The DAV and Periadriatic fault systems in the Eastern Alps south of the Tauern window. International Journal of Earth Sciences, 90. https://doi.org/10.1007/s005310000190

Márton E., Trajanova M., Zupančič N., Jelen B., 2006. Formation, uplift and tectonic integration of a Periadriatic intrusive complex (Pohorje, Slovenia) as reflected in magnetic parameters and palaeomagnetic directions. Geophysical Journal International, 167. https://doi.org/10.1111/j.1365-246X.2006.03098.x

Mitrović-Woodell I., Tesei T., Plan L., Habler G., Baroň I., Grasemann B., 2023. Deformation of columnar calcite within flowstone speleothem. Journal of Structural Geology, 174, 104924. https://doi.org/10.1016/j.jsg.2023.104924

Müller W., Prosser G., Mancktelow N.S., Villa I.M., Kelley S.P., Viola G., Oberli F., 2001. Geochronological constraints on the evolution of the Periadriatic Fault System (Alps). International Journal of Earth Sciences, 90. https://doi.org/10.1007/s005310000187

Nenna F., Aydin A., 2011. The formation and growth of pressure solution seams in clastic rocks: A field and analytical study. Journal of Structural Geology, 33, 633–643. https://doi.org/10.1016/j.jsg.2011.01.014

Ohl M., Plümper O., Chatzaras V., Wallis D., Vollmer C., Drury M., 2020. Mechanisms of fault mirror formation and fault healing in carbonate rocks. Earth and Planetary Science Letters, 530. https://doi.org/10.1016/j.epsl.2019.115886

Otsuki K., Monzawa N., Nagase T., 2003. Fluidization and melting of fault gouge during seismic slip: Identification in the Nojima fault zone and implications for focal earthquake mechanisms. Journal of Geophysical Research: Solid Earth, 108. https://doi.org/10.1029/2001JB001711

Passchier C.W., Trouw R.A.J., 2005. Deformation mechanisms. Springer, Berlin, Heidelberg, 2nd edition.

Payne, R. M., and Duan, B., 2016. Insights into pulverized rock formation from dynamic rupture models of earthquakes. Geophysical Journal International, 208, 715–723. https://doi.org/10.1093/gji/ggw436

Piane C., Clennell M.B., Keller J.V., Giwelli A., Luzin V., 2017. Carbonate hosted fault rocks: A review of structural and microstructural characteristic with implications for seismicity in the upper crust. Journal of Structural Geology, 103, 17–36. https://doi.org/10.1016/j.jsg.2017.09.003

Power W. L., Tullis T.E., 1989. The relationship between slickenside surfaces in fine-grained quartz and the seismic cycle. Journal of Structural Geology, 11, 879–893. https://doi.org/10.1016/0191-8141(89)90105-3

Pozzi G., Paola N.D., Nielsen S.B., Holdsworth R.E., Bowen L., 2018. A new interpretation for the nature and significance of mirror-like surfaces in experimental carbonate-hosted seismic faults. Geology, 46, 583–586. https://doi.org/10.1130/G40197.1

Ratschbacher L., Frisch W., Linzer H.G., 1991. Lateral extrusion in the Eastern Alps. Part 2: structural analysis. Tectonics, 10, 257–271. https://doi.org/10.1029/90TC02623

Rempe M., Mitchell T., Renner J., Nippress S., Ben-Zion Y., Rockwell T., 2013. Damage and seismic velocity structure of pulverized rocks near the San Andreas Fault. Journal of Geophysical Research: Solid Earth, 118/6, 2813–2831. https://doi.org/10.1002/jgrb.50184

Rempe M., Smith S.A., Ferri F., Mitchell T.M., Toro G.D., 2014. Clast-cortex aggregates in experimental and natural calcite-bearing fault zones. Journal of Structural Geology, 68, 142–157. https://doi.org/10.1016/j.jsg.2014.09.007

Renard F., Gratier J.P., Jamtveit B., 2000. Kinetics of crack-sealing, intergranular pressure solution, and compaction around active faults. Journal of Structural Geology, 22, 1395–1407. https://doi.org/10.1016/S0191-8141(00)00064-X

Renard F., Schmittbuhl J., Gratier J.P., Meakin P., Merino E., 2004. Three-dimensional roughness of stylolites in limestones. Journal of Geophysical Research, 109, 1–12. https://doi.org/10.1029/2003JB002555

Renner J., Rummel F., 1996. The effect of experimental and microstructural parameters on the transition from brittle failure to cataclastic flow of carbonate rocks. Tectonophysics, 258, 151–169. https://doi.org/10.1016/0040-1951(95)00192-1

Rowe C.D., Moore J.C., Meneghini F., McKeirnan A.W., 2005. Large-scale pseudotachylytes and fluidized cataclasites from an ancient subduction thrust fault. Geology, 33, 937–940. https://doi.org/10.1130/G21856.1

Rowe C.D., Kirkpatrick J.D., Brodsky E.E., 2012. Fault rock injections record paleo-earthquakes. Earth and Planetary Science Letters, 335–336, 154–166. https://doi.org/10.1016/j.epsl.2012.04.015

Rutter E.H., 1976. A Discussion on natural strain and geological structure – The kinetics of rock deformation by pressure solution. Philosophical Transactions of the Royal Society of London. Series A, Mathematical and Physical Sciences, 283, 203–219 https://doi.org/10.1098/rsta.1976.0079

Rutter E.H., 1983. Pressure solution in nature, theory and experiment. Journal of the Geological Society, 140, 725–740. https://doi.org/10.1144/gsjgs.140.5.0725

Rutter E., Hadizadeh J., 1991. On the influence of porosity on the low-temperature brittle-ductile transition in siliciclastic rocks. Journal of Structural Geology, 13, 609–614. https://doi.org/10.1016/0191-8141(91)90047-M

Sagy A., Korngreen D., 2012. Dynamic branched fractures in pulverized rocks from a deep borehole. Geology, 40/9, 799–802. https://doi.org/10.1130/G33194.1

Sala P., Bella P., Szczygieł J., Wróblewski W., Gradziński M., 2022. Healed speleothems: A possible indicator of seismotectonic activity in karst areas. Sedimentary Geology, 430, 106105. https://doi.org/10.1016/j.sedgeo.2022.106105

Sanders D., Ortner H., Pomella H., 2018. Stratigraphy and deformation of Pleistocene talus in relation to a normal fault zone (central Apennines, Italy). Sedimentary Geology, 373, 77–97. https://doi.org/10.1016/j.sedgeo.2018.05.013

Schmid S.M., Aebli H.R., Heller F., Zingg A., 1989. The role of the Periadriatic Line in the tectonic evolution of the Alps. Geological Society, London, Special Publications 1989, v.45; p153–171. https://doi.org/10.1144/gsl.sp.1989.045.01.08

Schönlaub H.P., Schuster R., 2015. Die zweigeteilten Karawanken und ihre erdgeschichtliche Entwicklung. Naturwissenschaftlicher Verein für Kärnten, Klagenfurt am Wörthersee.

Schröckenfuchs T., Bauer H., Grasemann B., Decker K., 2015. Rock pulverization and localization of a strike-slip fault zone in dolo-

mite rocks (Salzach-Ennstal-Mariazell-Puchberg fault, Austria). Journal of Structural Geology, 78, 57–85. https://doi.org/10.1016/j.jsg.2015.06.009

Schuck B., Janssen C., Schleicher A., Toy V., Dresen G., 2018. Microstructures imply cataclasis and authigenic mineral formation control geomechanical properties of New Zealand's Alpine Fault. Journal of Structural Geology, 110, 172–186. https://doi.org/10.1016/j.jsg.2018.03.001

Sibson R.H., 1977. Fault rocks and fault mechanisms. Journal of the Geological Society, 133, 191–213. https://doi.org/10.1144/gsjgs.133.3.0191

Siman-Tov S., Aharonov E., Sagy A., Emmanuel S., 2013. Nanograins form carbonate fault mirrors. Geology, 41, 703–706. https://doi.org/10.1130/G34087.1

Siman-Tov S., Aharonov E., Boneh Y., Reches Z., 2015. Fault mirrors along carbonate faults: Formation and destruction during shear experiments. Earth and Planetary Science Letters, 430, 367–376. https://doi.org/10.1016/j.epsl.2015.08.031

Smeraglia L., Bettucci A., Billi A., Carminati E., Cavallo A., Toro G.D., Natali M., Passeri D., Rossi M., Spagnuolo E., 2017. Microstructural evidence for seismic and aseismic slips along clay-bearing, carbonate faults. Journal of Geophysical Research: Solid Earth, 122, 3895–3915. https://doi.org/10.1002/2017JB014042

Smith S., Collettini C., Holdsworth R., 2008. Recognizing the seismic cycle along ancient faults: CO2-induced fluidization of breccias in the footwall of a sealing low-angle normal fault. Journal of Structural Geology, 30, 1034–1046. https://doi.org/10.1016/j.jsg.2008.04.010

Smith S.A.F., Billi A., Toro G.D., Spiess R., 2011. Principal slip zones in limestone: Microstructural characterization and implications for the seismic cycle (Tre Monti Fault, Central Apennines, Italy). Pure and Applied Geophysics, 168, 2365–2393. https://doi.org/10.1007/s00024-011-0267-5

Spötl C., Dublyansky Y., Koltai G., Racine T., Plan L., 2023. The Obir Caves adjacent to the Periadriatic Fault in southern Austria: Uplifted hypogene caves formed by carbonic acid speleogenesis. Geomorphology, Volume 441. https://doi.org/10.1016/j.geomorph.2023.108901

Sprenger W.L., 1996. Das Periadriatische Lineament südlich der Lienzer Dolomiten. Abhandlungen der Geologischen Bundesanstalt, Wien, 52, 1–220.

Suess E., 1901. Das Antlitz der Erde: 3, 1. Hälfte. Tempsky Freytag.

Sylvester A.G., 1988. Strike-slip faults. Geological Society of America Bulletin, 100, 1666–1703. https://doi.org/10.1130/0016-7606(1988)100<1666:SSF>2.3.CO;2

Szczygieł J., Gradziński M., Bella P., Hercman H., Littva J., Mendecki M.J., Sala P., Wróblewski W., 2021. Quaternary faulting in the Western Carpathians: Insights into paleoseismology from cave deformations and damaged speleothems (Demänová Cave System, Low Tatra Mts). Tectonophysics 820/2021, 229111. https://doi.org/10.1016/j.tecto.2021.229111

Tada R., Siever, R., 1989. Pressure solution during diagenesis. Annual Reviews of Earth and Planetary Sciences, 17., 89–118. https://doi.org/10.1146/annurev.ea.17.050189.000513

Tesei T., Carpenter B.M., Giorgetti C., Scuderi M.M., Sagy A., Scarlato P., Collettini C., 2017. Friction and scale-dependent deformation processes of large experimental carbonate faults. Journal of Structural Geology, 100, 12–23. https://doi.org/10.1016/j.jsg.2017.05.008

Thaler H., Solar E., Trimmel H., 1970. Höhlenplan der Wartburggrotte, Obir-Tropfsteinhöhlen. Archiv des Landesvereins für Höhlenkunde in Wien und Niederösterreich, Wien.

Tollmann A., 1977. Die Geologie von Österreich: Die Zentralalpen, volume 1. Deuticke, Wien.

Tschegg C., Hou Z., Rice A.H.N., Fendrych J., Matiasek E., Berger T., Grasemann B., 2020. Fault zone structures and strain localization in clinoptilolite-tuff (Nižný Hrabovec, Slovak Republic). Journal of Structural Geology, 138. https://doi.org/10.1016/j.jsg.2020.104090

Ujiie K., Yamaguchi A., Kimura G., Toh, S., 2007. Fluidization of granular material in a subduction thrust at seismogenic depths. Earth and Planetary Science Letters, 259, 307–318. https://doi.org/10.1016/j.epsl.2007.04.049

Verberne B.A., de Bresser J.H., Niemeijer A.R., Spiers C.J., de Winter D.M., Plümper O., 2013. Nanocrystalline slip zones in calcite fault gouge show intense crystallographic preferred orientation: Crystal plasticity at sub-seismic slip rates at 18–150 °C. Geology, 41/8, 863–866. https://doi.org/10.1130/G34279.1

Verberne B.A., Spiers C.J., Niemeijer A.R., Bresser J.H.P.D., Winter, D.A.M.D., Plümper O., 2014. Frictional properties and microstructure of calcite-rich fault gouges sheared at sub-seismic sliding velocities. Pure and Applied Geophysics, 171, 2617–2640. https://doi.org/10.1007/s00024-013-0760-0

Vignaroli G., Viola G., Diamanti R., Zuccari C., Garofalo P., Bonini S., Selli L., 2020. Multistage strain localisation and fluid-assisted cataclasis in carbonate rocks during the seismic cycle: Insights from the Belluno Thrust (eastern Southern Alps, Italy). Journal of Structural Geology, 141, 1–19. https://doi.org/10.1016/j.jsg.2020.104216

Viti C., Brogi A., Liotta D., Mugnaioli E., Spiess R., Dini A., Zucchi M., Vannuccini G., 2016. Seismic slip recorded in tourmaline fault mirrors from Elba Island (Italy). Journal of Structural Geology, 86, 1–12. https://doi.org/10.1016/j.jsg.2016.02.013

Vrabec M., Prešeren P.P., Stopar B., 2006. GPS study (1996–2002) of active deformation along the Periadriatic fault system in northeastern Slovenia: tectonic model. Geologica Carpathica, 57, 57–65.

Wechsler N., Allen E.E., Rockwell T.K., Girty G., Chester J.S., Ben-Zion Y., 2011. Characterization of pulverized granitoids in a shallow core along the San Andreas Fault, Littlerock, CA. Geophysical Journal International, 186/2, 401–417. https://doi.org/10.1111/j.1365-246X.2011.05059.x

Wilcox R., Hardingh T., Seely D.R., 1973. Basic wrench tectonics. American Association of Petroleum Geologists Bulletin, 57/1, 74–96. https://doi.org/10.1306/819A424A-16C5-11D7-8645000102C1865D

Woodcock N.H., Schubert C., 1994. Continental strike-slip tectonics. In Hancock P. L., editor, Continental deformation, 251–263. Pergamon Press, Oxford, 1st edition.

Woodcock N.H., Mort K., 2008. Classification of fault breccias and related fault rocks. Geological Magazine, 145, 435–440. https://doi.org/10.1017/S0016756808004883

Zhang X., Spiers C.J., Peach C.J., 2010. Compaction creep of wet granular calcite by pressure solution at 28°C to 150°C. Journal of Geophysical Research, 115, 1–18. https://doi.org/10.1029/2008JB005853

Received: 28.11.2024
Accepted: 15.5.2025
Editorial Handling: Kurt Stüwe